A bis-chelating (O^N^O)/(N^N) ligand for the synthesis of heterobimetallic Pt(II)/Re(I) complexes: tools for the optimization of a new class of Pt(II) anticancer agents.

Benoît Bertrand,[a]* Candice Botuha,[a] Jérémy Forté,[a] Héloïse Dossmann,[a] Michèle Salmain[a]

[a] Sorbonne Université, CNRS, Institut Parisien de Chimie Moléculaire (IPCM), F-75005 Paris, France

Corresponding author e-mail : benoit.bertrand@sorbonne-universite.fr

Abstract

The two independent (O^N^O) and (N^N) coordination sites of a newly synthesized bis 2-(hydroxyphenyl)-1,2,4-triazole platform have been exploited to prepare four monometallic neutral (O^N^O)Pt(II) complexes carrying DMSO, pyridine, triphenylphosphine or N-heterocyclic carbene (NHC) as fourth ligand. Then the second (N^N) coordination site was used to introduce an IR-active rhenium tricarbonyl entity, affording the four corresponding heterobimetallic neutral Pt(II)/Re(I) complexes as well as a cationic Pt(II)/Re(I) derivative. X-ray crystallographic studies showed that distortion of the organic platform occurred to accommodate the coordination geometry of both metal centers. No ligand exchange and no transchelation occurred upon incubation of the Pt(II) complexes in aqueous environment or in the presence of Fe(III), respectively. The ligand and the complexes antiproliferative activity was first screened on the triple negative breast cancer cell line MDA-MB-231. Then the IC_{50} of the most active candidates was determined on a wider panel of human cancer cells (MDA-MB-231, MCF-7 and A2780) as well as on a non-tumorigenic cell line (MCF-10A). Low micromolar activities were reached for the complexes carrying a DMSO ligand, making them the first examples of highly active though hydrolytically stable Pt(II) complexes. Finally, the characteristic mid-IR signature of the $Re(CO)_3$ fragment in the Pt/Re heterobimetallic complexes was used to quantify their uptake in breast cancer cells.

Introduction

Platinum complexes have been the standard of care for several types of cancers since *cis*diamminodichloridoplatinum(II) (cisplatin) was approved for clinical use at the end of the 70's.[1] However, resistances associated with heavy side effects have limited the scope of applicability of platinum-based chemotherapy.[2] The large majority of Pt(II) complexes that have further been tested as potential anticancer agents are all based on the model of cisplatin which is constituted by two water-exchangeable ligands in *cis* position and two stable ligands[3] in order to form intrastrand adducts with DNA.[4] Since these complexes have the same basic scaffold, they all suffer from the same limitations and trigger similar side effects to cisplatin causing, with the exceptions of oxaliplatin and carboplatin, their failure in clinical trials.[5] Thus, in order to overcome the limitations of cisplatin

and its derivatives, it seemed necessary to develop compounds with different mechanisms of action with respect to cisplatin. Several strategies have thus been explored including the replacement of platinum by other transition metals including Fe, Ru, Cu and Au.[6] We chose for our part to investigate other Pt(II) scaffolds which could act *via* different mechanisms and by then not suffer from the same shortcomings than cisplatin.

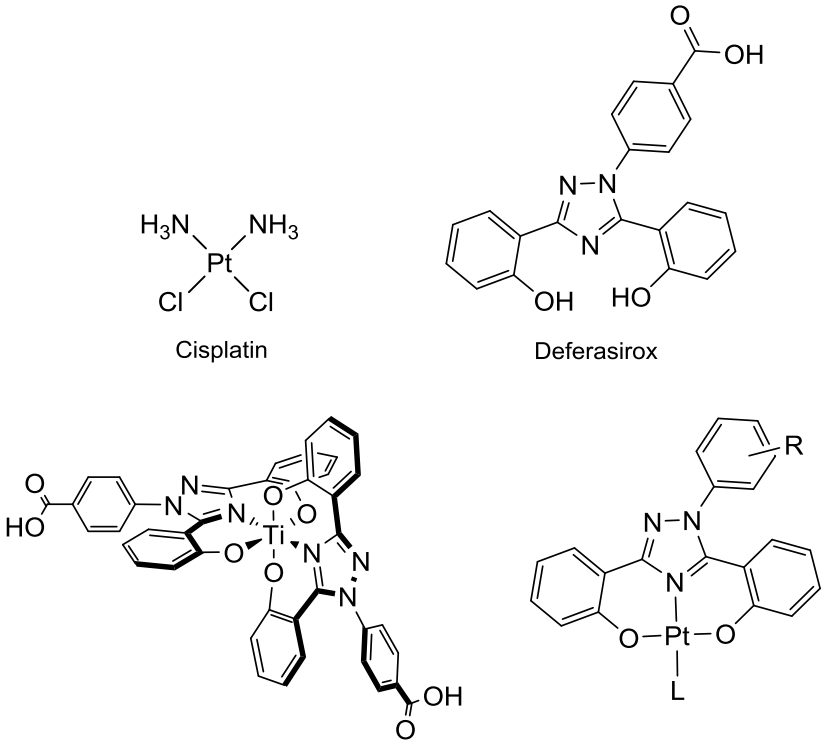

Figure 1: Structure of cisplatin, deferasirox and the deferasirox-based Ti(IV) and Pt(II) complexes.

4-[3,5-bis(2-hydroxyphenyl)-1,2,4-triazol-1-yl]benzoic acid (deferasirox, figure 1) is a well-known iron chelator used in the clinic to treat chronic iron overload.[7] Deferasirox and its derivatives are known to chelate metals in a (O^N^O) fashion and a Ti(IV) bis-deferasirox complex (figure 1) has been investigated for its anticancer properties. This complex owes its antiproliferative activity to a intracellular transchelation from titanium to iron.[8] Pt(II) complexes of deferasirox-like (O^N^O) ligands (figure 1) have also been investigated for their luminescence properties.[9]

Heterobimetallic complexes have been explored in the anticancer field in order to associate different metals within a single entity to enhance their activity. Several combinations have been tested with copper, gold, ruthenium, platinum or titanium.[10-14] Heterobimetallic complexes have also been developed for theranostic purposes by associating a biologically active metal with a metal-based luminophore such as ruthenium tris-bipyridine[15] and rhenium tris-carbonyl complexes.[16] Beyond their luminescence properties, rhenium-carbonyl complexes are also very interesting infrared (IR) reporter groups owing to their intense bands in the 2000 cm^{-1} spectral region where biological components hardly ever absorb.[17] In such a context, our group has introduced a methodology to measure the cellular uptake of compounds labeled by metal-carbonyl complexes by Fourier Transform (FT)-IR spectroscopy and has applied this methodology in the case of proteins,[18] organic[19] and organometallic[20] drugs.

In this context, we report herein the synthesis of a bis-chelating (O^N^O)/(N^N) ligand and the subsequent production of Pt(II) and heterobimetallic Pt(II)/Re(I) complexes. The structure and the absence of cross-resistance of these mono- and bimetallic complexes with cisplatin suggests a very different mechanism of action with respect to classical analogs of cisplatin. Taking advantage of the $Re(CO)_3$ fragment as IR probe, we were able to measure the cellular uptake of the heterobimetallic complexes. Combining these uptake data with partition coefficients (log $P_{o/w}$) and density functional theory (DFT) calculations enabled us to draw a structure-activity relationship for this new class of Pt(II) anticancer drug candidates. These data could be correlated to data obtained for very recently reported [(C^N^C)Pt(L)] complexes.[21]

Results and discussion

Synthesis and characterization

The bis-chelating (O^N^O)/(N^N) ligand LH_2 was synthesized in two steps by adapting the reported synthesis of 1,2,4-triazoles (scheme 1).[22] The first step consisted in the condensation of salicylamide with 2,4-dimethoxybenzoyl chloride to give the corresponding hydroxyphenylbenzoxazinone in 29 % yield. Then, upon reaction with 2-hydrazinopyridine first for 4 h at room temperature to open the benzoxazinone central ring followed by 2 h in refluxing ethanol to perform the cyclization affording the 1,2,4-triazole ring, the ligand LH_2 was obtained as a single regioisomer in 96 % yield.

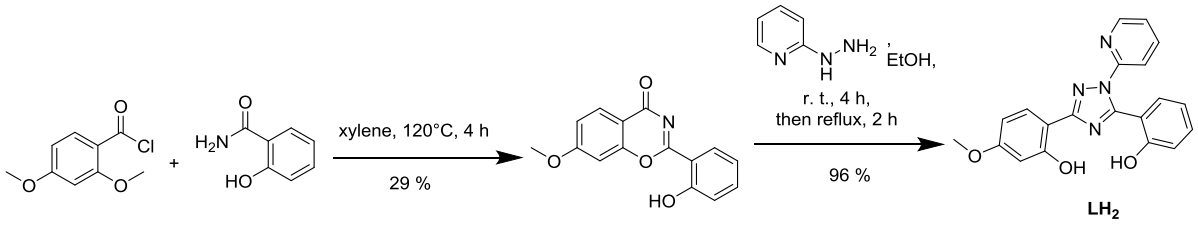

Scheme 1: Synthesis of the bis-chelating (O^N^O)/(N^N) ligand **LH_2**.

Selective coordination of platinum(II) ion in the (O^N^O) chelation site was achieved by reacting **LH_2** with $PtCl_2$ in the presence of K_2CO_3 in DMSO overnight at 60 °C. The corresponding platinum complex [LPt(DMSO)] **1a** was obtained in 84 % yield (scheme 2).

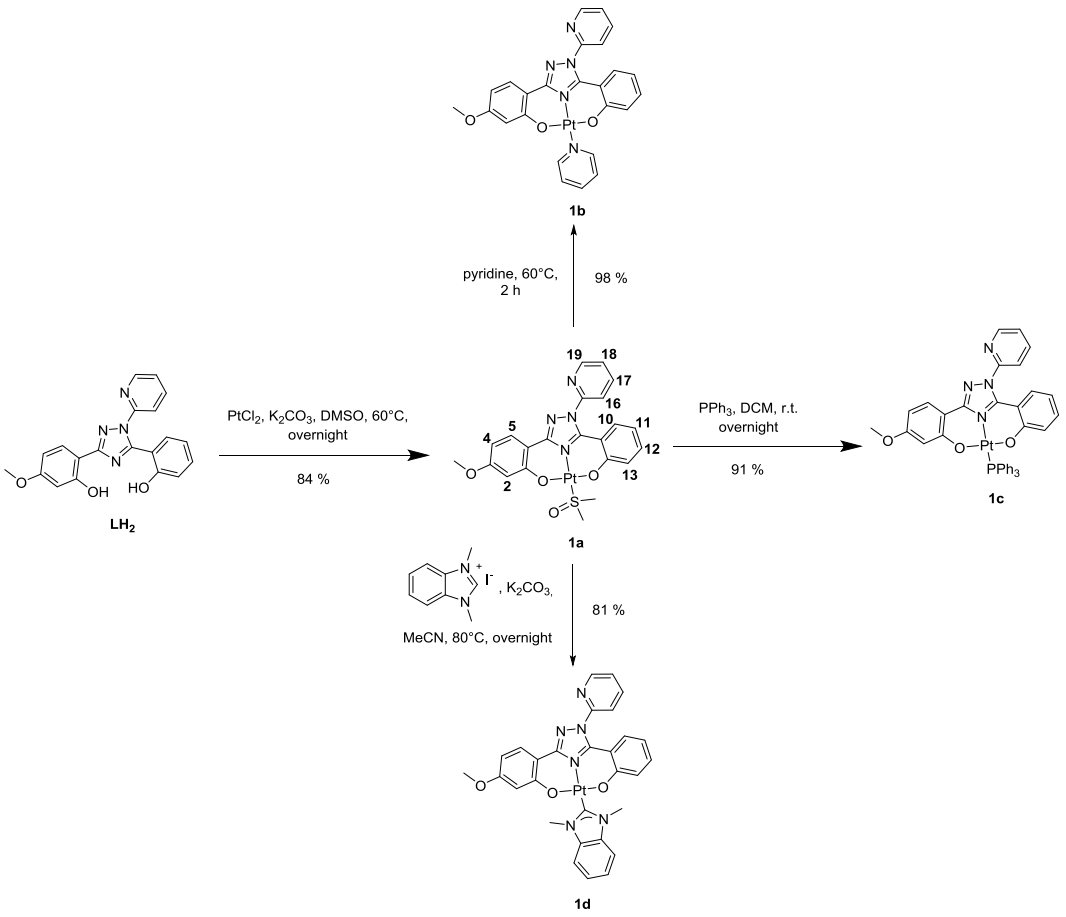

Scheme 2: Synthesis of the [(O^N^O)Pt(II)L] complexes **1a-d**.

Selective coordination of the Pt(II) ion in the (O^N^O) chelation site was assessed by ^{1}H nuclear magnetic resonance (NMR) spectroscopy by the disappearance of the signals corresponding to the two phenolic protons and the absence of a shift for the H^{19} signal (figure S10) ruling out the coordination of the pyridine ring. Moreover, the presence of one DMSO ligand was confirmed by ^{1}H NMR spectroscopy owing to the presence of a singlet at 3.40 ppm integrating for 6 protons. Compound **1a** could then be used as starting material to synthesize other Pt(II) complexes by replacing the DMSO ligand by pyridine to give complex **1b**, by triphenylphosphine to give complex **1c** and by 1,3-dimethylbenzimidazol-2-ylidene to give complex **1d** in 98 %, 91 % and 81 % yield, respectively (scheme 2). Substitution of DMSO was assessed by ^{1}H NMR spectroscopy in which the signal of the coordinated DMSO disappeared and was replaced by the signals of the coordinated pyridine, PPh_3 or NHC. In the case of **1c**, $^{31}P\{^{1}H\}$ NMR spectroscopy showed a signal at 9.61 ppm composed of a singlet and a small doublet with a coupling constant of 4189 Hz characteristic of the coordination of Pt(II).[23] In the case of **1d**, $^{13}C\{^{1}H\}$ NMR spectroscopy showed the signal of the carbenic carbon at 164.4 ppm which is in line with previously reported Pt(II)-NHC complexes.[24] The structure and purity of the compounds were assessed by high-resolution mass spectrometry (HRMS) and elemental analysis. Finally, all Pt(II) complexes were characterized by $^{195}Pt\{^{1}H\}$ NMR spectroscopy (figure 2). The chemical shift of the platinum center appeared to be highly sensitive to the nature of the monodentate ligand. It ranged between -1542 ppm for the pyridine complex **1b** and -2414 ppm for the PPh_3 complex **1c** (as a doublet due to the coupling with the phosphorous atom). These

chemical shift values are in good agreement with what has already been observed in the case of other (O^N^O)Pt(II) complexes.[25]

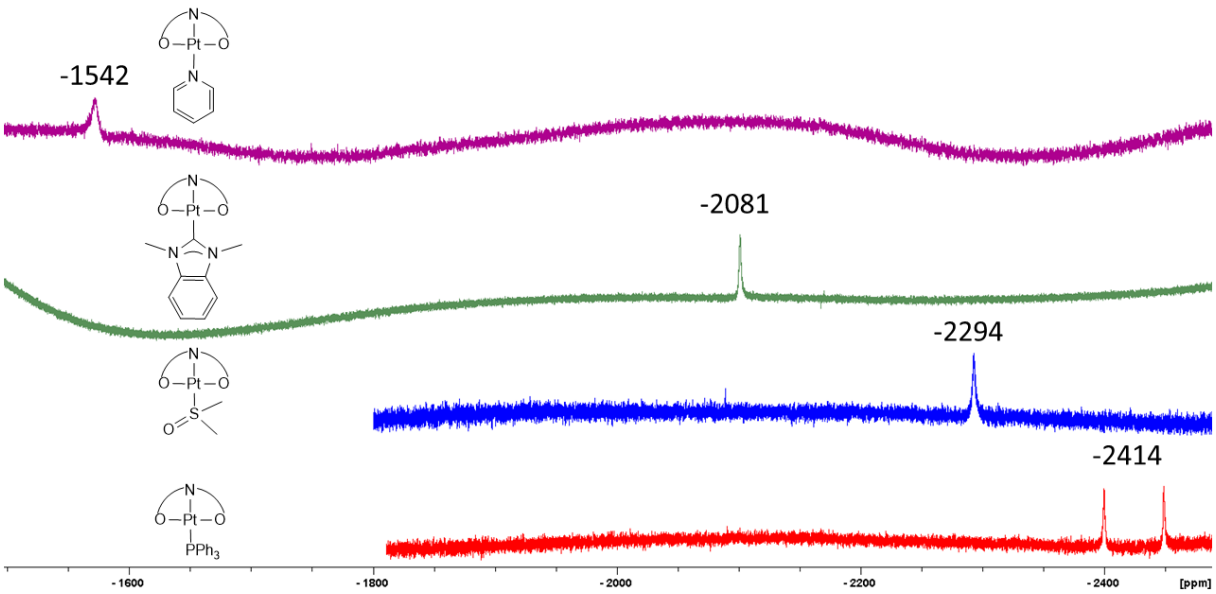

Figure 2: $^{195}Pt\{^{1}H\}$ NMR spectra of the (O^N^O)Pt(II) complexes **1a-d**.

We then took advantage of the remaining (N^N) chelation site to coordinate a $Re(CO)_3$ fragment which is well-known for its luminescence properties[26] and absorption properties in the mid-IR region.[19,20,27] All Pt(II) complexes were thus reacted with $[Re(CO)_5Br]$ in refluxing chloroform overnight following a reported procedure (scheme 3).[28] This led to the heterobimetallic Pt(II)/Re(I) complexes **2a-d** with yields ranging from 66 % to 95 %. The structure of the bimetallic complexes **2a-d** was assessed by ^{1}H NMR spectroscopy that showed a downfield shift of the H^{19} signal (see scheme 2 and figures S23 to S25 and S29 for atom labelling) from 8.7 ppm for **1a-d** to 9.0 ppm for **2a-d** typical of coordinated pyridines and a downfield shift of the H^5 signal from 8.0 ppm to 8.6 ppm. This shift came with the broadening of the H^5 signal for complexes **2a-d** due to the interactions with one CO of the $[BrRe(CO)_3]$ moiety. The bimetallic complexes were also characterized by IR spectroscopy showing in each case three vibration bands at 2027 (A'(1)), 1927 (A'(2)) and 1887 (A'') cm^{-1}, typical of $[(N^N)Re(CO)_3Br]$ complexes.[19,28] Complexes **2a** and **2b** were not soluble enough to record $^{13}C\{^{1}H\}$ and $^{195}Pt\{^{1}H\}$ NMR spectra, but $^{195}Pt\{^{1}H\}$ NMR spectra of complexes **2c** and **2d** were obtained and showed signals at -2454 and -2116 ppm respectively, very close to those observed in complexes **1c** and **1d**, thus suggesting a weak influence of the second metal on the chemical shift of the platinum center.

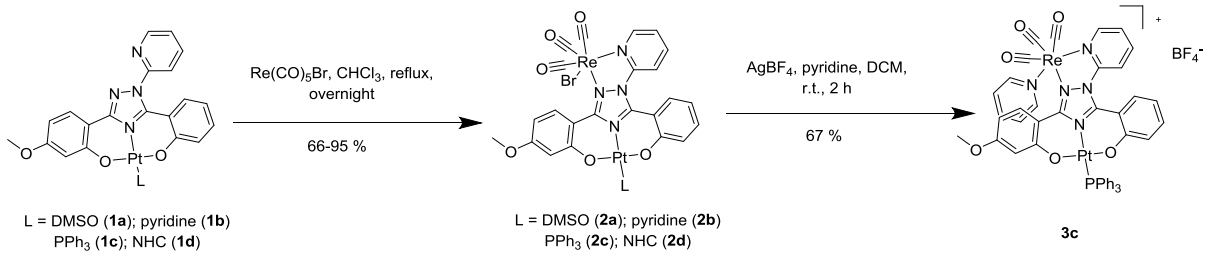

Scheme 3: Synthesis of the heterobimetallic Pt(II)/Re(I) complexes **2a-d** and **3c**.

We further functionalized one of the heterobimetallic complexes by replacing the bromido ligand on the Re(I) center in **2c** by a pyridine ligand to give **3c** as a BF_4^- salt. This was achieved at room temperature in the presence of silver tetrafluoroborate as bromide abstractor (scheme 3). The formation of complex **3c** was assessed by IR spectroscopy. A shift of the A'(1) band (2027 cm^{-1} for **2c**) to 2037 cm^{-1} and the merging of the two A'(2) and A'' bands (1927 and 1887 cm^{-1} for **2c**) into one broader band at 1923 cm^{-1} were observed, in agreement with previously reported works.[29] The structure of **3c** was further confirmed by ^{1}H, $^{13}C\{^{1}H\}$ NMR spectroscopy, HRMS and elemental analysis. As for the neutral heterobimetallic complex **2c**, the $^{195}Pt\{^{1}H\}$ NMR spectrum of **3c** shows a doublet centered at -2440 ppm confirming the poor influence of the coordination of the second metal on the chemical shift of the platinum center.

Surprisingly, although (diimine) Re(I) tris-carbonyl complexes are known to be emissive and are often used as luminescent probes as it has been reported for instance for Au(I)/Re(I) heterobimetallic systems,[30] all the Pt(II)/Re(I) heterobimetallic complexes appeared to be non-emissive. This quenching may be explained by the heavy atom effect due to the proximity of the Pt(II) center from the (N^N)$Re(CO)_3$ fragment.

Solid state structures

Single crystals suitable for X-Ray diffraction (XRD) analysis of complexes **1b**, **2a**, **2b**, **2c** and **3c** were grown by slow diffusion of pentane into a saturated solution of the compounds in dichloromethane at 4 °C. The crystal structures are depicted in figures 3 to 7 and crystallographic data are shown in table S3.

Note : Atoms numbering could be different between illustration of crystal structures and their CIF file available in CSD database.

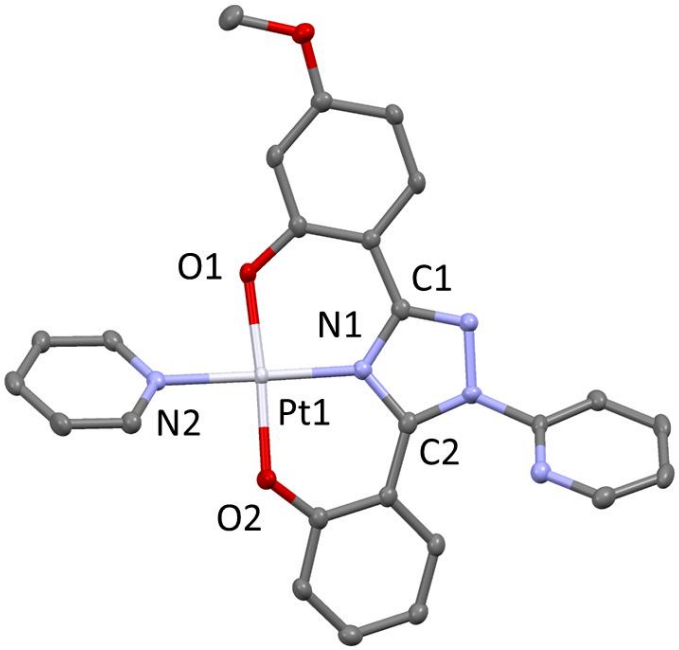

Figure 3: Crystal structure of complex **1b**. Ellipsoids set at 50% probability. Hydrogen atoms have been omitted for clarity. Selected bond distances [Å] and angles [°] measured at 140K: O_1-Pt_1 2.006(2), N_1-Pt_1 1.9962(3), O_2-Pt_1 2.003(2), N_2-Pt_1 2.033(3), O_1-Pt_1-N_1 92.55(9), O_1-Pt_1-N_2 88.96(9), O_2-Pt_1-N_1 91.41(9), O_2-Pt_1-N_2 89.12(9), O_1-Pt_1-O_2 175.97(8), N_1-Pt_1-N_2 177.40(10).

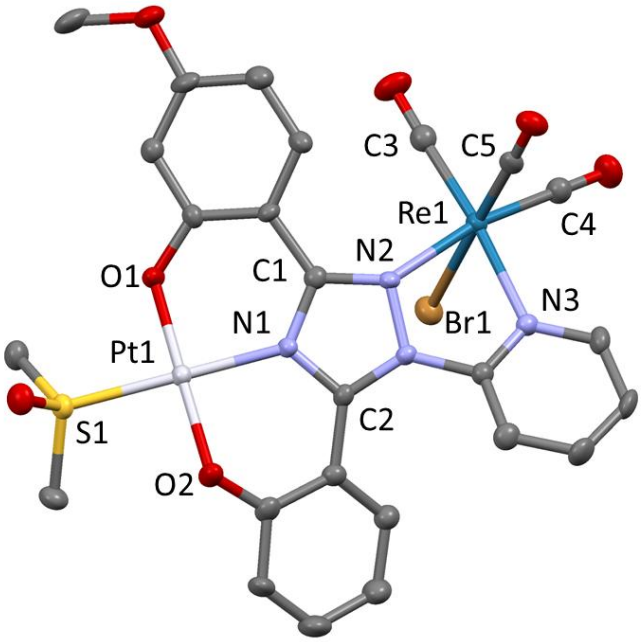

Figure 4: Crystal structure of heterobimetallic complex **2a**. Ellipsoids set at 50% probability. Hydrogen atoms and solvent molecule have been omitted for clarity. Selected bond distances [Å] and angles [°] measured at 200K: O_1-Pt_1 1.980(3), N_1-Pt_1 1.984(3), O_2-Pt_1 1.997(3), S_1-Pt_1 2.2166(11), N_3-Re_1 2.205(3), N_4-Re_1 2.187(3), C_4-Re_1 1.910(5), C_3-Re_1 1.926(5), C_5-Re_1 1.905(5), Br_1-Re_1 2.6253(5), O_1-Pt_1-N_1 90.09(13), O_1-Pt_1-S_1 88.92(9), O_2-Pt_1-N_1 89.19(13), O_2-Pt_1-S_1 91.75(10), O_1-Pt_1-O_2 178.43(12), N_1-

Pt_1-S_1 177.57(10), N_4-Re_1-N_3 74.08(13), N_3-Re_1-C_4 97.12(16), C_3-Re_1-C_4 87.50(19), N_4-Re_1-C_3 101.04(16), C_5-Re_1-Br_1 177.67(12), N_3-Re_1-C_4 169.91(15), N_4-Re_1-C_3 174.51(17).

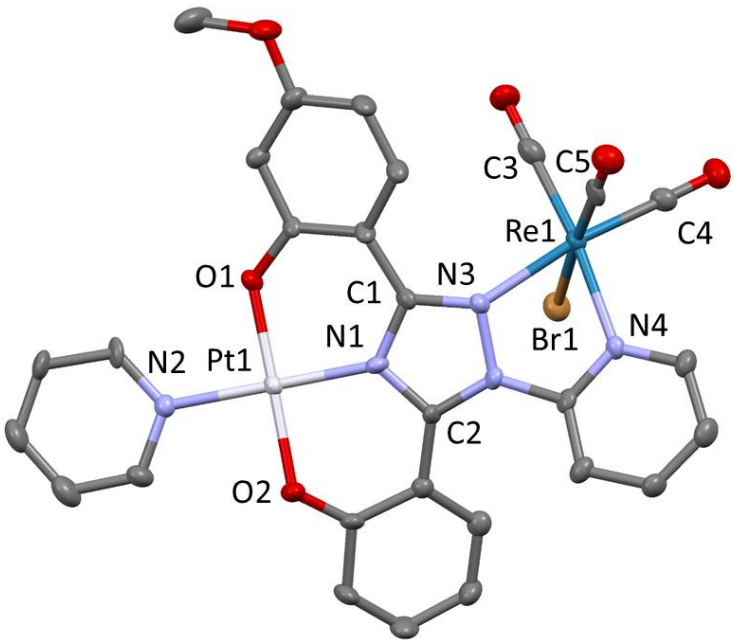

Figure 5: Crystal structure of heterobimetallic complex **2b**. Ellipsoids set at 50% probability. Hydrogen atoms and solvent molecules have been omitted for clarity. Selected bond distances [Å] and angles [°] measured at 150K: O_1-Pt_1 1.974(7), N_1-Pt_1 1.957(8), O_2-Pt_1 2.002(7), N_2-Pt_1 2.032(8), N_3-Re_1 2.201(8), N_4-Re_1 2.184(8), C_4-Re_1 1.891(11), C_3-Re_1 1.916(12), C_5-Re_1 1.920(12), Br_1-Re_1 2.6267(12), O_1-Pt_1-N_1 89.8(3), O_1-Pt_1-N_2 88.6(3), O_2-Pt_1-N_1 89.8(3), O_2-Pt_1-N_2 90.5(3), O_1-Pt_1-O_2 178.9(3), N_1-Pt_1-N_2 179.5(3), N_3-Re_1-N_4 73.2(3), N_4-Re_1-C_4 100.9(3), C_3-Re_1-C_4 85.2(5), N_3-Re_1-C_3 100.9(3), C_5-Re_1-Br_1 177.1(3), N_3-Re_1-C_4 171.0(4), N_4-Re_1-C_3 173.6(4).

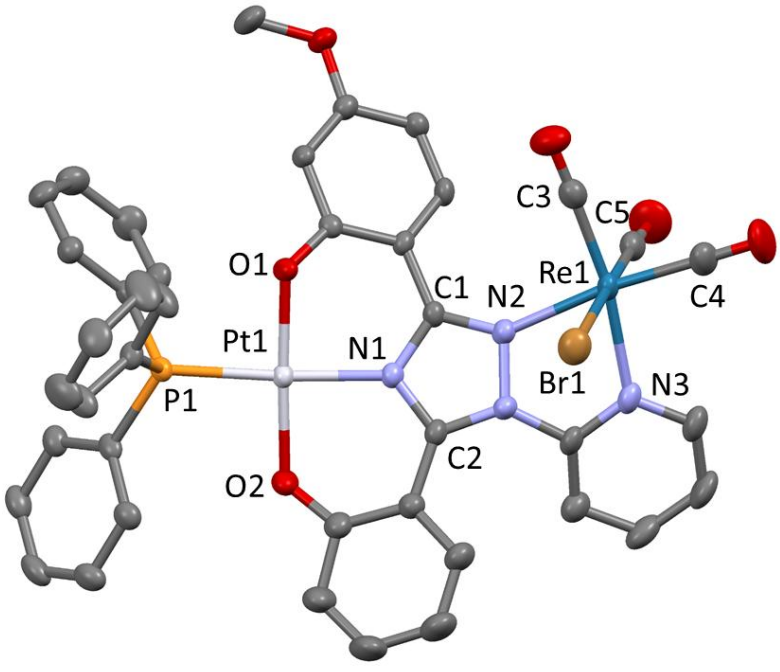

Figure 6: Crystal structure of heterobimetallic complex **2c**. Ellipsoids set at 50% probability. Br1 and carbonyl C5-O groups are disordered over two positions with an occupancy rate of 80/20. Hydrogen atoms, solvent molecules and the minor position of Br1/C5-O have been omitted for clarity. Selected bond distances [Å] and angles [°] measured at 200K: O_1-Pt_1 2.001(3), N_1-Pt_1 2.016(3), O_2-Pt_1 2.000(3), P_1-Pt_1 2.2449(10), N_2-Re_1 2.176(3), N_4-Re_1 2.189(4), C_4-Re_1 1.909(5), C_3-Re_1 1.929(5), C_5-Re_1 1.934(8), Br_1-Re_1 2.5906(7), O_1-Pt_1-N_1 87.28(8), O_1-Pt_1-P_1 89.15(12), O_2-Pt_1-N_1 88.54(13), O_2-Pt_1-P_1 95.04(9), O_1-Pt_1-O_2 177.64(11), N_1-Pt_1-P_1 176.40(10), N_2-Re_1-N_3 73.47(13), N_3-Re_1-C_4 99.89(19), C_3-Re_1-C_4 88.9(2), N_2-Re_1-C_3 97.64(16), C_5-Re_1-Br_1 177.6(3), N_2-Re_1-C_4 173.06(18), N_3-Re_1-C 170.55(16).

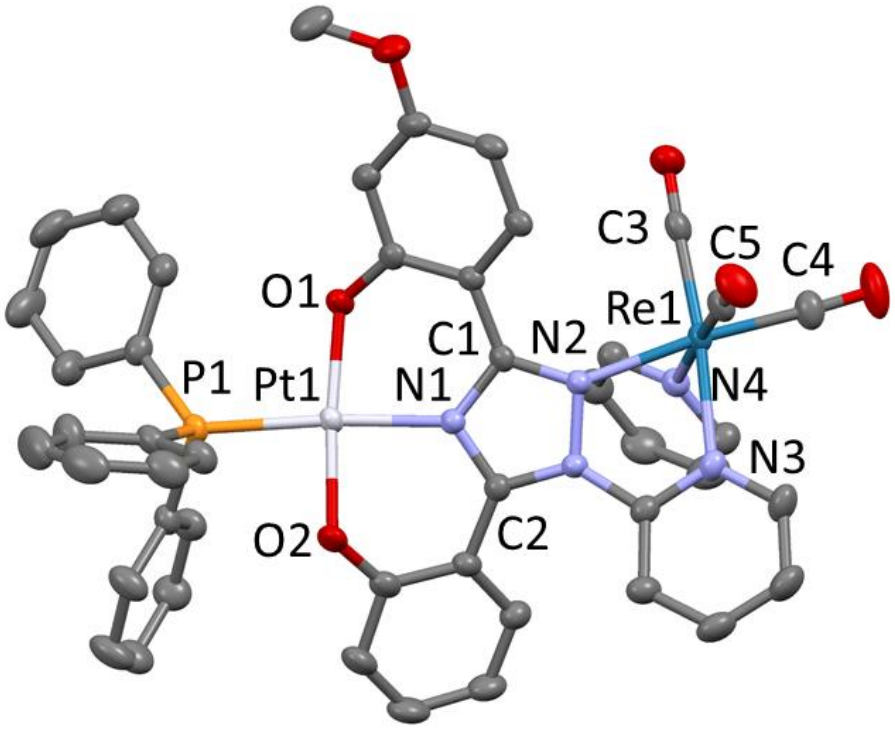

Figure 7: Crystal structure of heterobimetallic complex **3c**. Ellipsoids set at 50% probability. Hydrogen atoms, BF_4^- anion and solvent molecules have been omitted for clarity. Selected bond distances [Å] and angles [°] measured at 200K: O_1-Pt_1 2.0051(15), N_1-Pt_1 2.0225(18), O_2-Pt_1 2.0160(16), P_1-Pt_1 2.2633(6), N_2-Re_1 2.1816(18), N_4-Re_1 2.184(2), C_4-Re_1 1.915(3), C_3-Re_1 1.923(2), C_5-Re_1 1.920(2), N_4-Re_1 2.2167(19), O_1-Pt_1-N_1 87.03(7), O_1-Pt_1-P_1 97.35(5), O_2-Pt_1-N_1 88.26(7), O_2-Pt_1-P_1 87.36(3), O_1-Pt_1-O_2 175.28(6), N_1-Pt_1-P_1 175.62(5), N_2-Re_1-N_3 73.80(7), N_3-Re_1-C_4 100.38(10), C_3-Re_1-C_4 88.92(10), N_2-Re_1-C_3 100.89(8), C_5-Re_1-N_4 176.38(9), N_2-Re_1-C_4 173.67(10), N_3-Re_1-C_3 174.23(8).

All the structures show slightly distorted square-planar geometry for the platinum center, that is not affected by the presence of the rhenium(I) ion or by its coordination sphere. In the case of complex **2a**, DMSO appears to coordinate *via* its sulfur rather than its oxygen atom as previously reported.[31] For all heterobimetallic complexes, the Re(I) ion adopts a slightly distorted octahedral geometry. The main distortion arises from the bite angle of the (N^N) ligand (73 °) inducing a widening of the angles between the nitrogen atoms and the corresponding planar CO ligands (around 100 °). Moreover, a twist of the (O^N^O) ligand was noticed upon coordination of the Re(I) ion in **2b**. Data are summarized in table 1 and figure S1. When compared to an analog of complex **1b** (code CCDC

1058436)[9] in which the pyridine ring is replaced by a phenyl ring, we indeed observed an increase of the distortion of the (O^N^O) ligand by 10 ° (3.65 ° and 13.786 ° for CCDC 1058436 and **1b** respectively). Moreover, we observed an increase of the distortion of the (O^N^O) ligand upon coordination of the [$BrRe(CO)_3$] fragment by the (N^N) chelate (distortion angles of 27.625, 23.968 and 26.875 ° for **2a**, **2b** and **2c**). This increase happens to accommodate both coordination geometries of the Pt(II) and Re(I) centers while taking into account the steric hindrance between H^5 (according to ^1H NMR attribution) and one of the carbonyl ligands. These data confirm what we observed in solution by ^1H NMR spectroscopy. In the same way, increasing the bulkiness of the Re(I) fragment by replacing the bromido ligand by a pyridine induced a further increase of the distortion of the (O^N^O) ligand by 5 ° (distortion angles of 31.679 ° for **3c**).

Table 1: Absolute values of the O1-C1-C2-O2 distortion angle for complexes **1b**, **2a-c** and **3c** in comparison with a phenyl analog from literature.

Complexes	Absolute values of distortion angle O1-C1-C2-O2
CCDC 1058436[9]	3.650(111) °
1b	13.786(157)°
2a	27.625(212)°
2b	23.968(573)°
2c	26.875(213)°
3c	31.679(120)°

Notes: These values are measured by software Diamond[32]. XRD measurements of these compounds were performed at different temperatures between 140K and 200K. Thus, only large differences between these dihedral angle values, or very close values can be considered as significant.

Stability studies

In order to assess the outcome of the Pt(II) complexes in aqueous environment, all Pt(II) complexes **1a-d** (10^{-4} M) were incubated in an acetonitrile/water (1:1) mixture for 96 h at 37 °C and the corresponding UV-vis spectra were recorded at t = 0 and 96 h (figure 8 and S2-4). For complexes **1a**, **1b** and **1d** no change in the UV-vis spectra was noticed suggesting the very high stability of the [(O^N^O)PtL] scaffold in aqueous solution. However, concerning the highly lipophilic complex **1c**, a decrease of the intensity without any shift of the absorption bands was observed probably due to a lower solubility causing the precipitation of the complex during the incubation period. Moreover, considering that deferasirox-based [$(O^N^O)_2Ti$] complexes were demonstrated to be active due to metal exchange reaction with iron in the cells,[8] we recorded the UV-Vis spectra of each Pt(II) complex incubated with 10 equivalents of $FeCl_3$ (10^{-3} M) in the same acetonitrile/water (1/1) mixture immediately and after 96 h at 37 °C. At t = 0, all UV-vis spectra were identical to the mathematical addition of the spectrum of $FeCl_3$ at 10^{-3} M and the Pt(II) complex at 10^{-4} M, suggesting that no instantaneous reaction had occurred. Moreover, no change of the spectra of the mixture was noticed after 96 h for complexes **1a**, **1b** and **1d**. In the case of the mixture of **1c** and $FeCl_3$, a reduction of the intensity of the bands corresponding to **1c** was noticed, probably due to precipitation of the complex. All these data suggest that, conversely to what was previously observed in the case of the Ti(IV) deferasirox complexes, transchelation of Pt(II) by Fe(III) in complexes **1a-d** does not take place *in*

vitro and therefore may not take place *in cellulo* and that their mechanism of action may differ from that of titanium(IV).[8]

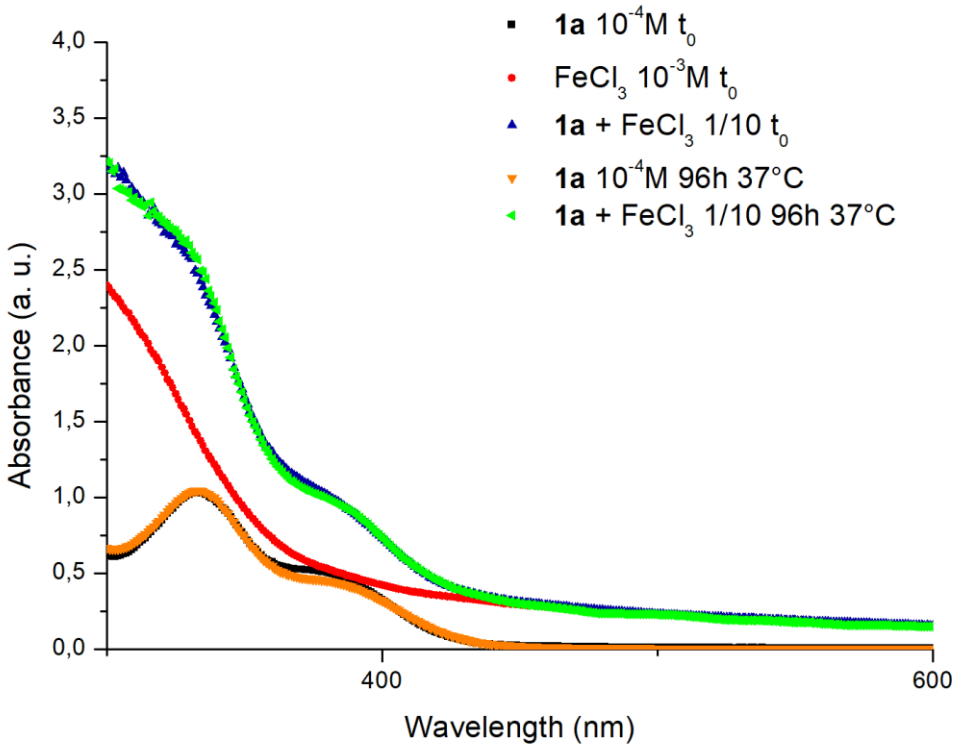

Figure 8: UV-Vis spectra of **1a** (10^{-4} M) alone or with 10 equivalents of Fe(III) (10^{-3} M) at t = 0 and 96 h in MeCN/H_2O 1:1 mixture at 37 °C.

In vitro antiproliferative activity and Log $P_{o/w}$ determination

Although the complexes proved to be only poorly soluble in purely aqueous media, all compounds were soluble enough in DMSO not to precipitate when diluted in aqueous buffer up to 100 µM with 1% DMSO. An initial screening of compounds **1a-d**, **2a-d** and **3c** was carried out on MDA-MB-231 triple negative human breast cancer cells. This cell line was chosen because platinum salts are currently the standard of care for this type of cancer although with variable outcome.[33] The inhibition of the proliferation of MDA-MB-231 cells was determined using the established MTT assay (see the experimental part for details) after 72 h of incubation with ligand **LH_2**, compounds **1a-d**, **2a-d** and **3c** and cisplatin at concentrations of 10 and 1 µM (figure 9).

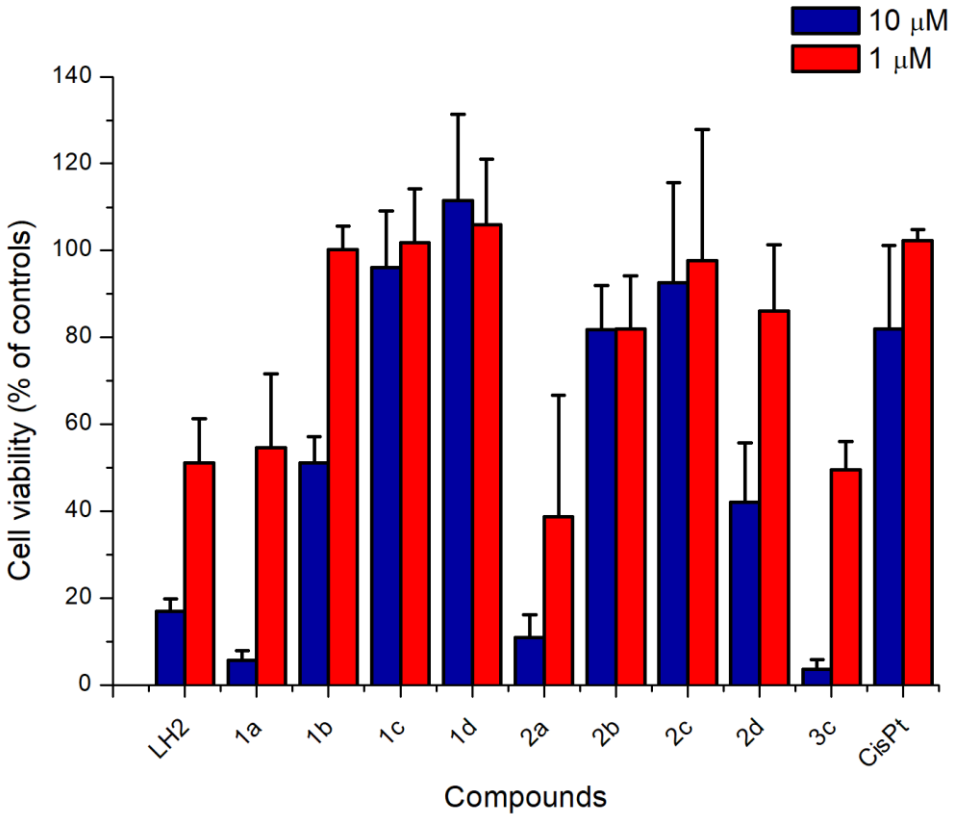

Figure 9: Inhibition of MDA-MB-231 cell growth by ligand **LH_2**, compounds **1a-d**, **2a-d** and **3c** and cisplatin; data represent the average ± standard error of three experiments.

Based on this preliminary screening, we applied an arbitrary threshold to exclude the less active molecules. This threshold was chosen so as to exclude complexes giving less than 50 % of reduction of cell viability at the concentration of 10 µM. This enabled us to select the five most promising candidates, being **LH_2**, **1a**, **2a**, **2d** and **3c**. This preliminary experiment highlighted the strong impact of the monodentate ligand on the cytotoxic activity of the compounds. Indeed, among all tested monometallic complexes, **1a** appeared to have a strong antiproliferative activity (cell viability of 5.7 ± 2.2 and 55 ± 17 % at 10 and 1 µM respectively) , **1b** showed a moderate activity (cell viability of 51 ± 6 % at 10 µM) whereas complexes **1c** and **1d** did not exhibit any activity even at the concentration of 10 µM. These data are consistent with the stability studies showing that no decoordination of the Pt(II) ion occurred, so that the toxicity of the complexes was not due to the release of the toxic ligand **LH_2**. In the neutral heterobimetallic series, the same trend seems to apply as well. Indeed, complex **2a** showed the strongest activity (cell viability of 10.8 ± 5.3 and 39 ± 25 % at 10 and 1 µM respectively), complexes **2b** and **2c** did not show any activity at both concentrations, however, complex **2d** showed some moderate activity (cell viability 42 ± 13 % at 10 µM). Finally, although neither monometallic complex **1c**, nor the corresponding heterobimetallic complex **2c** were active, the cationic heterobimetallic complex **3c** demonstrated strong antiproliferative activity (cell viability of 3.5 ± 2.3 and 59.5 ± 6.5 % at 10 and 1 µM respectively). This highlights the influence of the charge of the complex on the antiproliferative properties.

The five selected compounds and cisplatin were then tested for their half maximal inhibitory concentration (IC_{50}) after 72 h of incubation at 37 °C (with the concentration required for inhibition

of 50 % of cell proliferation) on a panel of human cancer cell lines including the triple negative breast cancer cell line MDA-MB-231, the ER-positive breast adenocarcinoma cell line MCF-7 and the ovarian carcinoma cell line A2780. The compounds were also tested on the healthy breast cell line MCF-10A for comparison. Results are summarized in table 2.

Table 2: Effect of compounds **LH_2**, **1a**, **2a**, **2d**, **3c** and cisplatin on cell viability of a panel of human cancerous and non-cancerous cell lines after 72 h of incubation at 37 °C and partition coefficients of all complexes; data represent the average ± standard error of three experiments.

Complex	IC_{50} ± sd (µM)				Log $P_{o/w}$
	MDA-MB-231	MCF-7	A2780	MCF-10A	
LH_2	0.7 ± 0.3	0.5 ± 0.2	1.4 ± 0.2	1.2 ± 0.2	4.10
1a	3.1 ± 0.5	1.6 ± 0.9	1.5 ± 0.6	1.1 ± 0.2	3.67
1b	n. d.	n. d.	n. d.	n. d.	3.34
1c	n. d.	n. d.	n. d.	n. d.	6.86
1d	n. d.	n. d.	n. d.	n. d.	4.50
2a	2.1 ± 0.6	2.2 ± 0.4	1.5 ± 0.3	1.82 ± 0.06	3.65
2b	n. d.	n. d.	n. d.	n. d.	4.87
2c	n. d.	n. d.	n. d.	n. d.	8.07
2d	9.2 ± 3.5	20.3 ± 1.9	34.5 ± 7.2	17.4 ± 2.6	5.81
3c	1.7 ± 0.3	1.1 ± 0.4	1.3 ± 0.2	3.3 ± 0.3	2.40
Cisplatin	20.4 ± 3.4	14 ± 3.5	1.0 ± 0.2	2.9 ± 0.8	n. d.

n.d.: not determined.

The deferasirox-based ligand **LH_2** appeared particularly cytotoxic with IC_{50} values down to submicromolar level being more than six times more active than deferasirox (IC_{50} = 4.4 ± 1.2 µM) on MDA-MB-231 cell line.[34] All tested complexes appeared more toxic than cisplatin toward the triple negative breast cancer cell line MDA-MB-231 and with the exception of **2d**, all complexes were also more toxic than cisplatin toward MCF-7 cell line. Moreover, the monometallic complex **1a** and the heterobimetallic complexes **2a** and **3c** showed IC_{50} values in the low micromolar range comparable with the one of cisplatin on the ovarian cancer cell line A2780. It is thus clear that there is no cross-resistance between these Pt(II) and Pt(II)/Re(I) complexes and cisplatin, suggesting a different mode of action with respect to cisplatin and to the free ligand **LH_2**. It is also worth noticing that no significant differences in the IC_{50} values of the monometallic complex **1a** and the corresponding neutral heterobimetallic complex Pt(II)/Re(I) **2a** are observed, suggesting that the cytotoxicity of the bimetallic complex mainly arises from the [(O^N^O)Pt(DMSO)] moiety. On the contrary, although neither the phosphine containing monometallic complex **1c** nor the corresponding neutral heterobimetallic complex **2c** did show any antiproliferative activity up to a concentration of 10 µM, the cationic heterobimetallic complex **3c** appeared to be the most toxic compound of the entire series (IC_{50} = 1.7 ± 0.3; 1.1 ± 0.4 and 1.3 ± 0.2 µM against MDA-MB-231, MCF-7 and A2780 cells respectively). This highlights the very strong impact of the $[(pyridine)Re(CO)_3]^+$ moiety on the cytotoxic properties of this bimetallic complex although cationic Re(I) complexes are not reported to be particularly active on lung cancer cells.[15a] However, when compared to the non-cancerous cell line MCF-10A, no particular selectivity for cancer cells was observed for the tested mono- and bimetallic complexes, which is also the case for cisplatin itself.

The partition coefficient values (Log $P_{o/w}$) were measured using a well-established chromatographic method.[35] The results are reported in table 2. We observed strong differences in the lipophilicity of

the monometallic complexes according to the nature of the ligands with the following trend: **1b** (pyridine) ≈ **1a** (DMSO) < **1b** (NHC) << **1c** (PPh_3). The neutral heterobimetallic complexes appeared slightly more lipophilic than their monometallic precursors and the trend observed in the monometallic series was maintained: **2a** < **2b** < **2d** << **2c**. This demonstrates the small modification of lipophilicity due to the addition of the [$Re(CO)_3$] fragment. The cationic heterobimetallic complex **3c** although bearing the PPh_3 ligand appeared the most hydrophilic complex of the entire family (log $P_{o/w}$ = 2.40) demonstrating the impact of the cationic charge in this case.

Theoretical study of the reactivity of the Pt(II) complexes

To investigate the reactivity of the [(O^N^O)PtL] scaffold, energetics parameters were calculated using DFT at the PBE0/ SDD(Pt),6-31g(d,p) (other atoms) level of theory. For Pt(II) complexes, ligand substitution reactions can occur *via* associative and dissociative mechanisms as depicted in scheme 4.

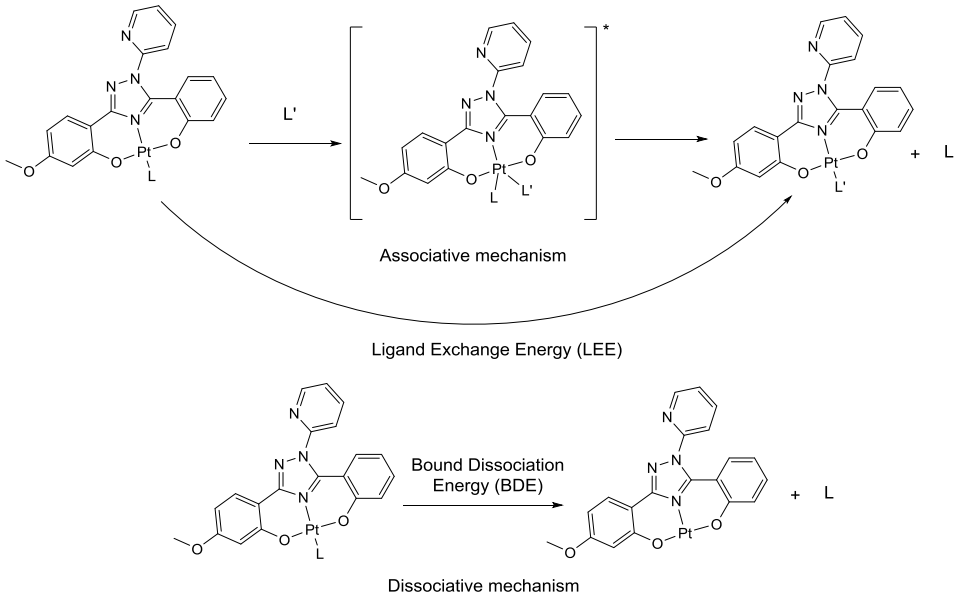

Scheme 4: Different mechanisms of ligand exchange reactions.

We calculated the ligand exchange energies considering both possible mechanisms for Pt(II) complexes **1a-d**. In the case of the associative mechanism, we chose H_2O, H_2S and imidazole as competitor ligands (L') and as models for biomolecules (water itself, alcohols, thiols, histidine and DNA bases). The results are presented in table 3. For the exchange of L by H_2O or H_2S, the ligand exchange energies (LEEs) were pretty similar ranging from 9.3 to 41.7 kcal/mol for **1a** and **1d** respectively. When imidazole was considered, the LEEs ranged from -7.7 to 24.7 kcal/mol. Overall, no matter which ligand was considered, the exchange reactions were the least energetic when L = DMSO, followed by pyridine and triphenylphosphine and the exchange reaction with NHC was by far the most energetic. The bond dissociation energies (BDE) corresponding to the loss of the monodentate ligand ranged from 42.1 kcal/mol up to 74.7 kcal/mol for complexes **1a** and **1b** respectively. DMSO thus appeared to be the most labile ligand followed by the pyridine and triphenylphosphine ligands which are quite similar and finally NHC turned to be the most strongly

bound ligand. Therefore, we can hypothesize that the reactivity scale of this series of compounds will be the following **1a** > **1b** > **1c** >> **1d**. Correlated with the IC_{50} data showing the DMSO complexes **1a** and **2a** as particularly effective, it seems that the lability of the monodentate ligand is required for the antiproliferative activity. A similar trend was noticed for a recently published series of neutral [(C^N^C)Pt(L)] complexes. Indeed, for a given (C^N^C) ligand, the corresponding complexes bearing the more labile MeCN ligand turned out to be more toxic than their counterparts carrying the DMSO ligand.[21] This suggests that the toxicity mechanism common to both (O^N^O) and (C^N^C)Pt(II)L complexes involves the direct coordination of Pt(II) to its biological target(s) by substitution of the ligand L.

Table 3: Ligand exchange energies and bond dissociation energies of the monodentate ligands for Pt(II) complexes **1a-d** (PBE0/Pt(SDD),6-31g(d,p) (other atoms)).

Complex	LEE, H_2O (kcal/mol)	LEE, H_2S (kcal/mol)	LEE, imidazole (kcal/mol)	BDE (kcal/mol)
1a	9.3	9.4	-7.7	42.3
1b	15.3	15.5	-1.6	48.4
1c	18.0	18.2	1.1	51.1
1d	41.7	41.8	24.7	74.7

Quantification of the cellular uptake of the heterobimetallic complexes by FT-IR

We quantified the amount of heterobimetallic complexes uptaken by MDA-MB-231 cells after 2 h of incubation at 37 °C in the presence of 50 µM of **2a-d** and **3c** following a protocol established in our group.[19,20,27] The intensity of the A' IR band at 2026 cm^{-1} in the IR spectra of a known number of cells treated with complexes **2a-d** and 2036 cm^{-1} in the IR spectrum of cells treated with complex **3c** was measured and the intracellular quantity of complexes **2a-d** and **3c** was deduced from calibration curves established for each complex (see experimental part for details). The results are depicted in figure 10.

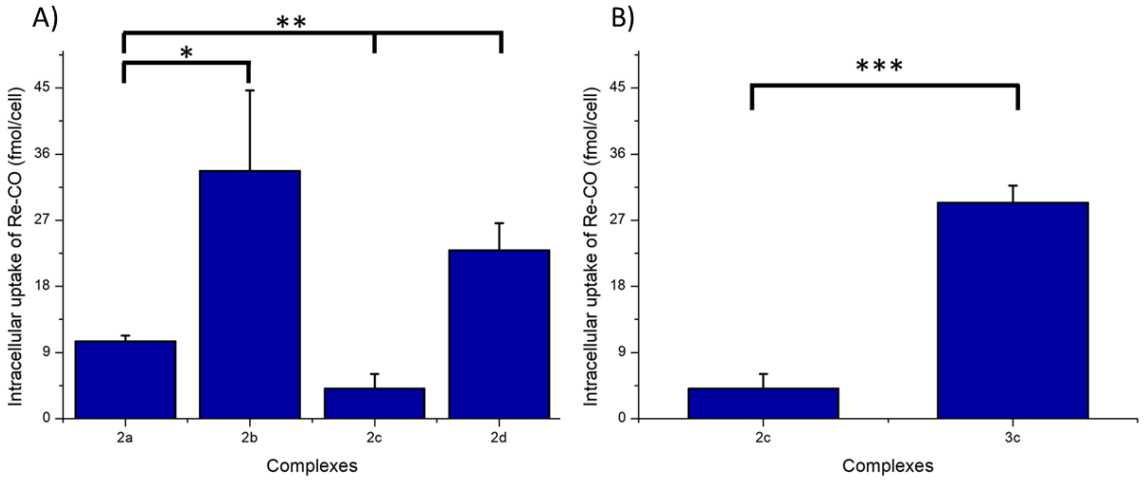

Figure 10: Intracellular uptake of complexes **2a-d** and **3c** in MDA-MB-231 cells after 2 h of incubation at 37 °C of A) neutral heterobimetallic complexes **2a-d** and B) PPh_3 containing complexes **2c** and **3c**;

data represent the average ± standard error of three experiments. The significance of the results was analyzed by t-test. *p value < 0.05; **p value < 0.01; ***p value < 0.001.

In the neutral complexes series (figure 10A), no clear correlation between the intracellular uptake values and the cytotoxicity could be established. Indeed, the most toxic compound **2a** (IC_{50} = 2.1 ± 0.6 µM) has only a moderate uptake (10.5 ± 0.8 fmol/cell) while the non- or moderately toxic complexes **2b** and **2d** present a much higher uptake (33.7 ± 11 and 22.9 ± 3.7 fmol/cell respectively). This suggests that the limiting factor may not be the cellular uptake but rather the intrinsic reactivity of the complexes within the cells. This type of behavior has already been observed for some cyclometallated Au(III) complexes carrying biotin or ethynylestradiol substituents.[36] Moreover, when plotting the uptake of the neutral complexes as a function of the partition coefficient (figure S5), we observe an optimum value of uptake for a log $P_{o/w}$ value around 5. Similar trends were observed in the case of [(C^N^C)Pt(L)] complexes.[21] This suggests that the cytotoxic properties of complexes **1a** and **2a** could be improved by increasing the lipophilicity of the complexes. This could be achieved either by replacing the DMSO ligand by a more lipophilic sulfoxide or by adding lipophilic substituent on the bis-chelating ligand.

As can be seen in figure 10B, the replacement of the bromido ligand in **2c** by a pyridine and the subsequent formation of the positively charged complex **3c** resulted in a seven-fold higher uptake in MDA-MB-231 cells. In this case, this increased uptake may account for the higher cytotoxic activity of **3c** with respect to **2c**. Such a correlation between IC_{50} and uptake has already been observed.[37] However, other parameters such as a different intracellular accumulation due to the positive charge should also be considered.

Conclusions

We synthesized a new bis-chelating ligand (O^N^O)/(N^N) based on the structure of the well-known iron chelator deferasirox. We selectively metallated the (O^N^O) chelation site with platinum and synthesized four different [(O^N^O)Pt(L)] complexes. We demonstrated the very strong influence of the ligand L on the electronic structure of the Pt(II) complexes by $^{195}Pt\{^{1}H\}$ NMR spectroscopy. We then synthesized five heterobimetallic Pt(II)/Re(I) complexes. These complexes were completely characterized including by X-Ray diffraction for complexes **1b**, **2a-c** and **3c**. We noticed a twist of the ligand to accommodate the coordination sphere of both metals. The Pt(II) complexes appeared to be stable in aqueous environment even in the presence of excess Fe(III) over a period of time of 96 h suggesting a mode of action which does not involve transchelation and iron depletion as it has previously been seen for closely related Ti(IV) complexes.[8] The *in vitro* antiproliferative screening enabled the selection of four complexes (**1a**, **2a**, **2d** and **3c**) as particularly promising. The best ones appeared 10 times more potent than cisplatin on naturally resistant cell lines suggesting a different mode of action. Thus, our study documents the extension of the scope of biologically active Pt(II) complexes. Finally, we took advantage of the specific IR signature of the $Re(CO)_3$ fragment to measure the cellular uptake of the heterobimetallic complexes. In the neutral complexes series, uptake seems not to be the main parameter responsible for the cytotoxicity, but rather the ease of dissociation of the monodentate ligand, the DMSO complexes **1a** and **2a** being the most active. Very

similar results were obtained with [(C^N^C)Pt(L)] complexes suggesting that (O^N^O)Pt and (C^N^C)Pt complexes may belong to the same class of platinum-based drugs.[21] We also observed an optimum uptake for complexes having a partition coefficient around 5. Altogether, the antiproliferative properties of our series of complexes result from a subtle interplay between ligand lability and cell uptake, the latter being directly correlated to lipophilicity and charge. This suggests that the activity of our (O^N^O)Pt complexes could be further increased by introducing a more labile nitrile ligand at the fourth coordination site or by enhancing the uptake of sulfoxido complexes by replacing the DMSO ligand by a more lipophilic sulfoxide ligand or by introducing lipophilic substituents on the (O^N^O) chelate. Mechanistic studies are currently ongoing in our lab to explore the mode of action of these new Pt(II) complexes.

Experimental part

General remarks

All reactions and manipulations were carried out under an argon atmosphere using standard Schlenk techniques. Anhydrous solvents were obtained by standard procedures. Chemicals were purchased from various manufacturers and used as received. ^{1}H, ^{13}C, ^{31}P and ^{195}Pt NMR spectra were acquired on a Bruker 400 MHz spectrometer. Chemical shifts (δ) are expressed as ppm referenced to the solvent residual signal. Splitting patterns are expressed as follows: s, singlet; d, doublet; t, triplet; m, multiplet. Mass spectrometry was carried out at the HRMS facility of Sorbonne Université (Paris). High resolution mass spectra (HR-MS) were recorded on a LTQ-Orbitrap XL mass spectrometer (Thermo Scientific, San Jose, CA, USA) IR spectra were recorded on a Tensor 27 FT-IR spectrometer (Bruker). Elemental analysis was performed at the elemental analysis service of ICSN (Gif-sur-Yvette, France).

Synthesis

Synthesis of **2-(2-hydroxyphenyl)-7-methoxy-4H-benzo[e][1,3]oxazin-4-one**

In a round bottom flask **salicylamide** (2.04 g, 14.8 mmol) and **2,4-dimethoxybenzoyl chloride** (3.86 g, 19.3 mmol) were suspended in xylene (40 mL). The reaction was heated to 120°C for 4 h leading to the complete dissolution of the starting materials and to the coloration of the solution in yellow. After the reaction mixture has been cooled down to room temperature, xylene was evaporated under reduced pressure. The obtained crude product was washed with Et_2O and triturated with a EtOAc/cyclohexane mixture three times to give after drying under vacuum the pure product as a beige powder (1.13 g, 4.22 mmol, 29 % yield). ^{1}H NMR ($CDCl_3$, 400 MHz, 298 K): δ 13.02 (broad s, 1 H, OH), 8.18 (dd, $^{3}J_{H\text{-}H}$ = 7.8 Hz, $^{4}J_{H\text{-}H}$ = 1.5 Hz, 1 H, H^{13}), 7.99 (d, $^{3}J_{H\text{-}H}$ = 9.0 Hz, 1 H, H^{5}), 7.76 (m, 1 H, H^{10}), 7.47 (m, 2 H, H^{11} + H^{12}), 6.57 (dd, $^{3}J_{H\text{-}H}$ = 8.9 Hz, $^{4}J_{H\text{-}H}$ = 2.5 Hz, 1 H, H^{4}), 6.53 (d, $^{4}J_{H\text{-}H}$ = 2.4 Hz, 1 H, H^{5}), 3.87 (s, 3 H, OMe). ^{13}C{^{1}H} Jmod ($CDCl_3$, 100 MHz, 298 K): δ 167.0 (s, *C*^{3}), 165.8 (s, *C*^{7}), 165.2 (s, *C*^{6}), 164.0 (s, *C*^{14}), 154.2 (s, *C*^{9}), 135.5 (s, *C*^{10}), 130.2 (s, *C*), 128.0 (s, *C*^{5}), 126.9 (s, *C*^{13}), 118.4 (s, *C*^{8}), 116.9 (s, *C*$^{11/12}$), 109.2 (s, *C*^{4}), 104.2 (s, *C*^{1}), 101.3 (s, *C*^{2}), 55.9 (s, *C*H$_3$). ESI-MS (MeCN) *positive mode exact mass* for $[C_{15}H_{11}NO_4Na]^+$ (292.0580): measured *m/z* 292.0581 $[M+Na]^+$.

Synthesis of **2-(3-(2-hydroxyphenyl)-1-(pyridin-2-yl)-1H-1,2,4-triazol-5-yl)-5-methoxyphenol** (**LH_2**)

In a round-bottom flask **2-(2-hydroxyphenyl)-7-methoxy-4H-benzo[e][1,3]oxazin-4-one** (1.13 g, 4.22 mmol), **2-hydrazinopyridine** (461 mg, 4.22 mmol) and **triethylamine** (650 µL, 4.65 mmol) were added in EtOH (110 mL). The reaction was stirred at room temperature for 4 h and then at reflux for 1 h. After the reaction mixture has been cooled down to room temperature, water (150 mL) was added and EtOH was removed under reduced pressure. After pH adjustment to 6 with AcOH, the product was extracted with DCM (3 x 150 mL). The organic phase was dried over $MgSO_4$, filtered and after evaporation of DCM and drying under vacuum, the pure product was obtained as a brown powder (1.45 g, 4.04 mmol, 96 % yield). ^{1}H NMR ($CDCl_3$, 400 MHz, 298 K): δ 11.23 (broad s, 1 H, OH), 9.84 (s, 1 H, 2 OH), 8.60 (dd, $^3J_{H-H}$ = 4.8 Hz, $^4J_{H-H}$ = 1.2 Hz, 1 H, H^{19}), 8.02 (m, 2 H, H^5 + H^{17}), 7.67 (d, $^3J_{H-H}$ = 8.0 Hz, 1 H, H^{16}), 7.50 (ddd, $^3J_{H-H}$ = 7.4 Hz, $^3J_{H-H}$ = 4.9 Hz, $^4J_{H-H}$ = 0.6 Hz, 1 H, H^{18}), 7.34 (ddd, $^3J_{H-H}$ = 8.6 Hz, $^3J_{H-H}$ = 7.4 Hz, $^4J_{H-H}$ = 1.6 Hz, 1 H, H^{11}), 7.12 (dd, $^3J_{H-H}$ = 8.4 Hz, $^4J_{H-H}$ = 1.0 Hz, 1 H, H^{10}), 6.97 (dd, $^3J_{H-H}$ = 8.0 Hz, $^4J_{H-H}$ = 1.5 Hz, 1 H, H^{13}), 6.71 (ddd, $^3J_{H-H}$ = 8.2 Hz, $^3J_{H-H}$ = 7.3 Hz, $^4J_{H-H}$ = 1.1 Hz, 1 H, H^{12}), 6.60 (m, 2 H, H^2 + H^4), 3.85 (s, 3 H, OMe). $^{13}C\{^1H\}$ Jmod ($CDCl_3$, 100 MHz, 298 K): δ 162.8 (s, C^3), 159.7 (s, C^6), 158.4 (s, C^1), 157.9 (s, C^9), 152.6 (s, C^{14}), 150.9 (s, C^{15}), 149.3 (s, C^{19}), 139.8 (s, C^{17}), 133.0 (s, C^{11}), 128.8 (s, C^5), 128.7 (s, C^{13}), 125.1 (s, C^{18}), 120.7 (s, C^{16}), 119.2 (s, C^{12}), 118.7 (s, C^{10}), 111.6 (s, C^8), 107.4 (s, C^4), 106.5 (s, C^7), 101.6 (s, C^2), 55.6 (s, CH_3). ESI-MS (MeCN) *positive mode exact mass* for $[C_{20}H_{17}N_4O_3]^+$ (361.1295): measured *m/z* 361.1295 $[M+H]^+$.

Synthesis of **[(L)Pt(DMSO)]** (**1a**)

In a round-bottom flask **2-(3-(2-hydroxyphenyl)-1-(pyridin-2-yl)-1H-1,2,4-triazol-5-yl)-5-methoxyphenol** (300 mg, 0.83 mmol) was dissolved into DMSO (15 ml) with **$PtCl_2$** (222 mg, 0.83 mmol) and **K_2CO_3** (346 mg, 2.50 mmol). The reaction was maintained at 60°C overnight. After addition of brine (75 mL), the formed yellow precipitate was extracted three times with DCM and the organic phase was washed three times with water and dried over $MgSO_4$. After partial removal under vacuum of DCM, the product was precipitated with cyclohexane, dried and obtained pure as a yellow powder (440 mg, 0.70 mmol, 84 % yield). ^{1}H NMR ($CDCl_3$, 400 MHz, 298 K): δ 8.65 (ddd, $^3J_{H-H}$ = 4.8 Hz, $^4J_{H-H}$ = 1.8 Hz, $^5J_{H-H}$ = 0.7 Hz, 1 H, H^{19}), 7.99 (ddd, $^3J_{H-H}$ = 7.8 Hz, $^3J_{H-H}$ = 7.8 Hz, $^4J_{H-H}$ = 1.9 Hz, 1 H, H^{17}), 7.95 (d, $^3J_{H-H}$ = 8.9 Hz, 1 H, H^5), 7.63 (d, $^3J_{H-H}$ = 8.0 Hz, 1 H, H^{16}), 7.52 (ddd, $^3J_{H-H}$ = 7.6 Hz, $^3J_{H-H}$ = 4.8 Hz, $^4J_{H-H}$ = 0.9 Hz, 1 H, H^{18}), 7.13 (ddd, $^3J_{H-H}$ = 8.5 Hz, $^3J_{H-H}$ = 6.9 Hz, $^4J_{H-H}$ = 1.1 Hz, 1 H, H^{11}), 7.00 (dd, $^3J_{H-H}$ = 8.6 Hz, $^4J_{H-H}$ = 1.8 Hz, 1 H, H^{10}), 6.68 (dd, $^3J_{H-H}$ = 8.3 Hz, $^4J_{H-H}$ = 1.6 Hz, 1 H, H^{13}), 6.45 (d, $^4J_{H-H}$ = 2.5 Hz, 1 H, H^2), 6.37 (ddd, $^3J_{H-H}$ = 8.2 Hz, $^3J_{H-H}$ = 6.9 Hz, $^4J_{H-H}$ = 1.2 Hz, 1 H, H^{12}), 6.32 (dd, $^3J_{H-H}$ = 8.9 Hz, $^4J_{H-H}$ = 2.5 Hz, 1 H, H^4), 3.78 (s, 3 H, OMe), 3.40 (s, 6 H, DMSO). $^{13}C\{^1H\}$ Jmod NMR ($CDCl_3$, 100 MHz, 298 K): δ 165.1 (s, C^{14}), 163.6 (s, C^1), 162.6 (s, C^3), 151.9 (s, C^6), 151.6 (s, C^{15}), 149.9 (s, C^{19}), 145.9 (s, C^9), 139.6 (s, C^{17}), 132.5 (s, C^{11}), 128.8 (s, C^5), 128.4 (s, C^{13}), 125.3 (s, C^{18}), 122.7 (s, C^{10}), 121.1 (s, C^{16}), 116.1 (s, C^{12}), 110.1 (s, C^8), 106.3 (s, C^4), 105.6 (s, C^7), 103.1 (s, C^2), 55.3 (s, OCH_3), 40.7 (s, (O)S(CH_3)$_2$). $^{195}Pt\{^1H\}$ NMR ($CDCl_3$, 86 MHz, 298 K): δ -2294 (s, (L2)*Pt*(DMSO)). ESI-MS (MeCN) *positive mode exact mass* for $[C_{22}H_{20}N_4O_4SPtNa]^+$ (654.0745): measured *m/z* 654.0752 $[M+Na]^+$. IR υ_{max} (neat/cm^{-1}): 1115 (S=O). Calcd for $C_{22}H_{20}N_4O_4SPt.0.1C_6H_{12}$ (638.4): C, 42.41; H, 3.34; N, 8.75; S, 5.01. Found: C, 42.48; H 3.53; N 8.58; S, 4.90.

Synthesis of **[(L)Pt(pyridine)]** (**1b**)

In a round-bottom flask **[(L)Pt(DMSO)]** (50 mg, 0.079 mmol) was suspended in pyridine (5 ml). The reaction was maintained at 50°C for 2 h leading to the complete dissolution of the starting material. After cooling down to room temperature, pyridine was evaporated under vacuum. The formed oily solid was dissolved into DCM and rinsed with water three times and dried over $MgSO_4$. After partial removal of DCM under vacuum, the product was precipitated with cyclohexane, dried and obtained pure as a yellow powder (49 mg, 0.077 mmol, 98 % yield). ^{1}H NMR ($CDCl_3$, 400 MHz, 298 K): δ 9.12 (d, $^3J_{H\text{-}H}$ = 5.5 Hz, 2 H, H^{20}), 8.67 (broad s, 1 H, H^{19}), 7.95 (m, 3 H, H^5 + H^{17}, H^{22}), 7.63 (d, $^3J_{H\text{-}H}$ = 7.8 Hz, 2 H, H^{16}), 7.50 (m, 3 H, H^{18} + H^{21}), 7.13 (t, $^3J_{H\text{-}H}$ = 7.7 Hz, 2 H, H^{11}), 7.05 (d, $^3J_{H\text{-}H}$ = 8.5 Hz, 2 H, H^{10}), 6.69 (d, $^3J_{H\text{-}H}$ = 8.2 Hz, 2 H, H^{13}), 6.52 (d, $^3J_{H\text{-}H}$ = 1.8 Hz, 2 H, H^2), 6.32 (m, 2 H, H^4 + H^{12}), 3.79 (s, 3 H, OMe). $^{13}C\{^1H\}$ Jmod NMR ($CDCl_3$, 100 MHz, 298 K): δ 165.4 (s, C^{14}), 164.3 (s, C^1), 162.3 (s, C^3), 152.6 (s, C^6), 152.0 (s, C^{15}), 149.9 (s, C^{19}), 149.1 (s, C^{20}), 145.6 (s, C^9), 139.5 (s, C^{17}), 138.3 (s, C^{22}), 131.9 (s, C^{11}), 128.8 (s, C^5), 128.3 (s, C^{13}), 125.1 (s, C^{18}), 125.0 (s, C^{21}), 122.7 (s, C^{10}), 121.3 (s, C^{16}), 115.6 (s, C^{12}), 110.5 (s, C^8), 106.2 (s, C^7), 105.8 (s, C^4), 102.9 (s, C^2), 55.3 (s, OCH$_3$). $^{195}Pt\{^1H\}$ NMR ($CDCl_3$, 86 MHz, 298 K): δ -1542 (s, (L2)*Pt*(pyridine)). ESI-MS (MeCN) *positive mode exact mass* for $[C_{25}H_{19}N_5O_3PtNa]^+$ (655.1028): measured *m/z* 655.1036 $[M+Na]^+$. Calcd for $C_{25}H_{19}N_5O_3Pt$ (632.5): C, 47.47; H, 3.03; N, 11.07. Found: C, 47.86; H 3.41; N 10.66.

Synthesis of **[(L)Pt(PPh$_3$)]** (**1c**)

In a round-bottom flask **[(L)Pt(DMSO)]** (200 mg, 0.32 mmol) and **PPh$_3$** (83 mg, 0.32 mmol) were dissolved in DCM (10 mL). The reaction was kept at room temperature overnight. DCM (10 mL) was added and the organic phase was washed three times with water (20 mL). After drying over $MgSO_4$ and partial evaporation of DCM, cyclohexane was added leading to the formation of a yellow precipitate. After filtration and drying the pure product was obtained as a yellow powder (238 mg, 0.29 mmol, 91 % yield). ^{1}H NMR ($CDCl_3$, 400 MHz, 298 K): δ 8.65 (ddd, $^3J_{H\text{-}H}$ = 4.8 Hz, $^4J_{H\text{-}H}$ = 1.8 Hz, $^5J_{H\text{-}H}$ = 0.7 Hz, 1 H, H^{19}), 7.98 (d, $^3J_{H\text{-}H}$ = 8.9 Hz, 1 H, H^5), 7.93 (dt, $^3J_{H\text{-}H}$ = 7.7 Hz, $^4J_{H\text{-}H}$ = 1.9 Hz, 1 H, H^{17}), 7.84 (m, 6 H, H^{21}), 7.60 (d, $^3J_{H\text{-}H}$ = 7.8 Hz, 1 H, H^{16}), 7.48 (m, 10 H, H^{18} + H^{22} +H^{23}), 6.98 (ddd, $^3J_{H\text{-}H}$ = 8.6 Hz, $^3J_{H\text{-}H}$ = 6.9 Hz, $^4J_{H\text{-}H}$ = 1.8 Hz, 1 H, H^{11}), 6.71 (dd, $^3J_{H\text{-}H}$ = 8.2 Hz, $^4J_{H\text{-}H}$ = 1.6 Hz, 1 H, H^{10}), 6.48 (dd, $^3J_{H\text{-}H}$ = 8.6 Hz, $^4J_{H\text{-}H}$ = 1.0 Hz, 1 H, H^{13}), 6.30 (ddd, $^3J_{H\text{-}H}$ = 8.2 Hz, $^3J_{H\text{-}H}$ = 6.9 Hz, $^4J_{H\text{-}H}$ = 1.2 Hz, 1 H, H^{12}), 6.26 (dd, $^3J_{H\text{-}H}$ = 8.9 Hz, $^4J_{H\text{-}H}$ = 2.6 Hz, 1 H, H^4), 5.93 (d, $^4J_{H\text{-}H}$ = 2.5 Hz, 1 H, H^2), 3.66 (s, 3 H, OMe). $^{13}C\{^1H\}$ Jmod NMR ($CDCl_3$, 100 MHz, 298 K): δ 166.0 (s, C^{14}), 164.6 (s, C^1), 162.0 (s, C^3), 152.7 (s, C^6), 151.9 (s, C^{15}), 149.8 (s, C^{19}), 146.6 (s, C^9), 139.4 (s, C^{17}), 134.7 (d, $^2J_{P\text{-}C}$ = 10.9 Hz, C^{21}), 131.8 (s, C^{11}), 130.8 (d, $^4J_{P\text{-}C}$ = 2.4 Hz, C^{23}), 128.7 (s, C^5), 128.6 (d, $^1J_{P\text{-}C}$ = 60.5 Hz, C^{20}), 128.5 (s, C^{13}), 128.3 (d, $^3J_{P\text{-}C}$ = 11.0 Hz, C^{22}), 124.9 (s, C^{18}), 123.1 (s, C^{10}), 121.0 (s, C^{16}), 115.3 (s, C^{12}), 111.0 (s, C^8), 106.6 (s, C^7), 105.2 (s, C^4), 103.7 (s, C^2), 55.0 (s, OCH$_3$). $^{31}P\{^1H\}$ NMR ($CDCl_3$, 162 MHz, 298 K): δ 9.61 (s + d, $^1J_{P\text{-}Pt}$ = 4189 Hz, PPh_3). $^{195}Pt\{^1H\}$ NMR ($CDCl_3$, 86 MHz, 298 K): δ -2414 (d, $^1J_{P\text{-}Pt}$ = 4214 Hz, (L2)*Pt*(PPh_3)). ESI-MS (MeCN) *positive mode exact mass* for $[C_{38}H_{29}N_4O_3PPtH]^+$ (816.1698): measured *m/z* 816.1701 $[M+H]^+$. Calcd for $C_{38}H_{29}N_4O_3PPt.0.5C_6H_{12}$ (857.8): C, 57.41; H, 4.11; N, 6.53. Found: C, 57.25; H 4.23; N 6.28.

Synthesis of **[(L)Pt(1,3-dimethylbenzimidazol-2-ylidene)]** (**1d**)

In a round-bottom flask **[(L)Pt(DMSO)]** (200 mg, 0.32 mmol), **1,3-dimethylbenzimidazolium iodide** (87 mg, 0.32 mmol) and **K$_2$CO$_3$** (88 mg, 0.64 mmol) were dissolved in acetonitrile (20 mL). The

reaction was kept at 80 °C overnight. Acetonitrile was removed under reduced pressure, DCM (50 mL) was added and the organic phase was washed three times with water (50 mL). After drying over $MgSO_4$ and partial evaporation of DCM, cyclohexane was added leading to the formation of a yellow precipitate. After filtration and drying the pure product was obtained as a yellow powder (181 mg, 0.26 mmol, 81 % yield). ^{1}H NMR ($CDCl_3$, 400 MHz, 298 K): δ 8.67 (d, $^3J_{H\text{-}H}$ = 3.7 Hz, 1 H, H^{19}), 8.05 (d, $^3J_{H\text{-}H}$ = 8.8 Hz, 1 H, H^5), 7.97 (t, $^3J_{H\text{-}H}$ = 7.9 Hz, 1 H, H^{17}), 7.65 (d, $^3J_{H\text{-}H}$ = 8.0 Hz, 1 H, H^{16}), 7.49 (dd, $^3J_{H\text{-}H}$ = 7.1 Hz, $^3J_{H\text{-}H}$ = 5.2 Hz, 1 H, H^{18}), 7.45 (m, 2 H, H^{22}), 7.36 (m, 2 H, H^{23}), 7.12 (ddd, $^3J_{H\text{-}H}$ = 8.4 Hz, $^3J_{H\text{-}H}$ = 6.8 Hz, $^4J_{H\text{-}H}$ = 1.3 Hz, 1 H, H^{12}), 6.92 (d, $^3J_{H\text{-}H}$ = 8.2 Hz, 1 H, H^{13}), 6.78 (dd, $^3J_{H\text{-}H}$ = 8.3 Hz, $^4J_{H\text{-}H}$ = 1.4 Hz, H^{10}), 6.31-6.39 (m, 3 H, H^2 + H^4 + H^{11}), 4.31 (s, 6 H, NMe), 3.75 (s, 3 H, OMe).). $^{13}C\{^1H\}$ Jmod NMR ($CDCl_3$, 100 MHz, 298 K): δ 165.7 (s, C^{14}), 164.4 (s, $C^{1/20}$), 164.3 (s, $C^{1/20}$), 162.1 (s, C^3), 152.8 (s, C^6), 151.9 (s, C^{15}), 149.7 (s, C^{19}), 146.2 (s, C^9), 139.3 (s, C^{17}), 134.9 (s, C^{21}), 131.8 (s, C^{12}), 128.8 (s, C^5), 128.6 (s, C^{13}), 124.8 (s, C^{18}), 123.4 (s, C^{23}), 122.4 (s, C^{10}), 121.0 (s, C^{16}), 115.4 (s, C^{11}), 111.3 (s, C^8), 110.2 (s, C^{22}), 106.8 (s, C^7), 105.1 (s, C^4), 103.2 (s, C^2), 55.0 (s, OCH$_3$), 33.5 (s, NCH$_3$). $^{195}Pt\{^1H\}$ NMR ($CDCl_3$, 86 MHz, 298 K): δ -2081 (s, (L2)*Pt*(NHC)). ESI-MS (MeCN) *positive mode exact mass* for $[C_{29}H_{24}N_6O_3PtH]^+$ (700.1630): measured *m/z* 700.1635 $[M+H]^+$. Calcd for $C_{29}H_{24}N_6O_3Pt$ (699.6): C, 49.79; H, 3.46; N, 12.01. Found: C, 49.84; H 3.84; N 11.22.

Synthesis of **$[Br(CO)_3Re(L)Pt(DMSO)]$** (**2a**)

In a round-bottom flask **[(L)Pt(DMSO)]** (50 mg, 0.079 mmol) and **$Re(CO)_5Br$** (32 mg, 0.079 mmol) were dissolved in chloroform (5 mL). The reaction was refluxed overnight. After the reaction mixture has been cooled down to room temperature, chloroform was evaporated partially under reduced pressure and upon addition of diethylether the product precipitated which led after drying under vacuum to the pure product as a yellow-orange powder (74 mg, 0.075 mmol, 95 % yield). ^{1}H NMR ($CDCl_3$, 400 MHz, 298 K): δ 9.01 (d, $^3J_{H\text{-}H}$ = 4.6 Hz, 1 H, H^{19}), 8.56 (broad s, 1 H, H^5), 7.98 (ddd, $^3J_{H\text{-}H}$ = 8.7 Hz, $^3J_{H\text{-}H}$ = 7.5 Hz, $^4J_{H\text{-}H}$ = 1.6 Hz, 1 H, H^{17}), 7.71 (d, $^3J_{H\text{-}H}$ = 8.5 Hz, 1 H, H^{16}), 7.49 (ddd, $^3J_{H\text{-}H}$ = 7.4 Hz, $^3J_{H\text{-}H}$ = 5.6 Hz, $^4J_{H\text{-}H}$ = 1.0 Hz, 1 H, H^{18}), 7.42 (dd, $^3J_{H\text{-}H}$ = 8.3 Hz, $^4J_{H\text{-}H}$ = 1.4 Hz, 1 H, H^{10}), 7.37 (ddd, $^3J_{H\text{-}H}$ = 8.6 Hz, $^3J_{H\text{-}H}$ = 6.9 Hz, $^4J_{H\text{-}H}$ = 1.6 Hz, 1 H, H^{12}), 7.15 (dd, $^3J_{H\text{-}H}$ = 8.7 Hz, $^4J_{H\text{-}H}$ = 0.7 Hz, 1 H, H^{13}), 6.68 (ddd, $^3J_{H\text{-}H}$ = 8.1 Hz, $^3J_{H\text{-}H}$ = 6.9 Hz, $^4J_{H\text{-}H}$ = 1.1 Hz, 1 H, H^{11}), 6.58 (dd, $^3J_{H\text{-}H}$ = 9.1 Hz, $^4J_{H\text{-}H}$ = 2.5 Hz, 1 H, H^4), 6.47 (d, $^4J_{H\text{-}H}$ = 2.5 Hz, 1 H, H^2), 3.82 (s, 3 H, OMe), 3.42 (s, 3 H, S(O)Me), 3.40 (s, 3 H, S(O)Me). Due to solubility limitations, no $^{13}C\{^1H\}$ or $^{195}Pt\{^1H\}$ NMR spectra could be recorded. ESI-MS (MeCN) *positive mode exact mass* for $[C_{25}H_{20}N_4O_7SBrPtReNa]^+$ (1004.9314): measured *m/z* 1004.9303 $[M+Na]^+$. Calcd for $C_{25}H_{20}N_4O_7SBrPtRe$ (981.7): C, 30.59; H, 2.05; N, 5.71; S, 3.27. Found: C, 30.72; H, 2.02; N, 5.65; S, 2.75. IR υ_{max} (neat/cm^{-1}): 2027 (C≡O), 1927 (C≡O), 1887 (C≡O), 1147 (S=O).

Synthesis of **$[Br(CO)_3Re(L)Pt(pyridine)]$** (**2b**)

In a round-bottom flask **[(L)Pt(pyridine)]** (50 mg, 0.079 mmol) and **$Re(CO)_5Br$** (32 mg, 0.079 mmol) were dissolved in chloroform (5 mL). The reaction was refluxed overnight. After the reaction mixture has been cooled down to room temperature, chloroform was partially evaporated under reduced pressure and upon addition of diethylether the product precipitated which lead after drying under vacuum to the pure product as a yellow-orange powder (58 mg, 0.059 mmol, 74 % yield). ^{1}H NMR ($CDCl_3$, 400 MHz, 298 K): 9.02 (d, $^3J_{H\text{-}H}$ = 5.2 Hz, 2 H, H^{20}), 8.99 (d, $^3J_{H\text{-}H}$ = 5.4 Hz, 1 H, H^{19}), 8.64 (broad

s, 1 H, H^5), 7.99 (t, $^3J_{H-H}$ = 7.6 Hz, 1 H, H^{22}), 7.94 (dt, $^3J_{H-H}$ = 8.1 Hz, $^4J_{H-H}$ = 1.8 Hz, 1 H, H^{17}), 7.68 (d, $^3J_{H-H}$ = 8.6 Hz, 1 H, H^{16}), 7.57 (t, $^3J_{H-H}$ = 7.1 Hz, 2 H, H^{21}), 7.36-7.47 (m, 3 H, H^{10} + H^{11} + H^{18}), 7.17 (d, $^3J_{H-H}$ = 8.3 Hz, 1 H, H^{13}), 6.64 (t, $^3J_{H-H}$ = 7.4 Hz, 1 H, H^{12}), 6.56 (m, 2 H, H^2 + H^4), 3.84 (s, 3 H, OMe). Due to solubility limitations, no $^{13}C\{^1H\}$ or $^{195}Pt\{^1H\}$ NMR spectra could be recorded. Calcd for $C_{28}H_{19}N_5O_6BrPtRe$ (982.7): C, 34.22; H, 1.95; N, 7.13. Found: C, 34.17; H 2.12; N 7.00. IR υ_{max} (neat/cm^{-1}): 2025 (C≡O), 1927 (C≡O), 1888 (C≡O).

Synthesis of **$[Br(CO)_3Re(L)Pt(PPh_3)]$** (**2c**)

In a round-bottom flask **$[(L)Pt(PPh_3)]$** (40 mg, 0.048 mmol) and **$Re(CO)_5Br$** (20 mg, 0.048 mmol) were dissolved in chloroform (1 mL). The reaction was refluxed overnight. After the reaction mixture has been cooled down to room temperature, chloroform was partially evaporated under reduced pressure and upon addition of cyclohexane the product precipitated which lead after drying under vacuum to the pure product as an orange powder (37 mg, 0.032 mmol, 66 % yield). ^1H NMR ($CDCl_3$, 400 MHz, 298 K): δ 8.98 (d, $^3J_{H-H}$ = 3.3 Hz, 1 H, H^{19}), 8.57 (broad s, 1 H, H^5), 7.92 (ddd, $^3J_{H-H}$ = 8.4 Hz, $^3J_{H-H}$ = 7.6 Hz, $^4J_{H-H}$ = 1.6 Hz, 1 H, H^{17}), 7.77 (m, 6 H, H^{22}), 7.65 (d, $^3J_{H-H}$ = 8.5 Hz, 1 H, H^{16}), 7.54 (m, 3 H, H^{23}), 7.38-7.49 (m, 8 H, H^{10} + H^{18} + H^{22}), 7.20 (ddd, $^3J_{H-H}$ = 8.6 Hz, $^3J_{H-H}$ = 7.0 Hz, $^4J_{H-H}$ = 1.6 Hz, 1 H, H^{12}), 6.58 (m, 2 H, H^{11} + H^{13}), 6.49 (dd, $^3J_{H-H}$ = 9.1 Hz, $^4J_{H-H}$ = 2.6 Hz, 1 H, H^4), 5.87 (d, $^4J_{H-H}$ = 2.6 Hz, 1 H, H^2), 3.67 (s, 3 H, OMe). $^{13}C\{^1H\}$ Jmod NMR ($CDCl_3$, 100 MHz, 298 K): δ 195.2 (s, *C*≡O), 194.5 (s, *C*≡O), 169.9 (s, C^{14}), 168.9 (s, C^1), 164.4 (s, C^3), 153.1 (s, C^{19}), 150.1 (s, C^{15}), 148.8 (s, C^6 + C^9), 140.0 (s, C^{17}), 135.0 (s, C^{11}), 134.6 (d, $^2J_{P-C}$ = 11.1 Hz, C^{21}), 131.3 (s, C^{23}), 129.3 (s, C^{10}), 128.6 (d, $^3J_{P-C}$ = 11.0 Hz, C^{22}), 127.6 (d, $^1J_{P-C}$ = 62.3 Hz, C^{20}), 124.7 (s, C^{13}), 124.4 (s, C^{18}), 116.9 (s, C^{12} + C^{16}), 109.9 (s, C^8), 106.9 (s, C^4), 104.5 (s, C^2), 104.1 (s, C^7), 55.2 (s, O*C*H_3), C^5 not visible. $^{31}P\{^1H\}$ NMR ($CDCl_3$, 162 MHz, 298 K): δ 8.59 (s + d, $^1J_{P-Pt}$ = 4295 Hz, PPh_3). $^{195}Pt\{^1H\}$ NMR ($CDCl_3$, 86 MHz, 298 K): δ -2454 (d, $^1J_{P-Pt}$ = 4310 Hz, $Br(CO)_3Re(L2)$*Pt*(PPh_3)). ESI-MS (MeCN) *positive mode exact mass* for $[C_{41}H_{29}N_4O_6PBrPtReNa]^+$ (1189.0064): measured *m/z* 1189.0091 $[M+Na]^+$. Calcd for $C_{41}H_{29}N_4O_6PPtReBr.0.25C_6H_{12}$ (1186.9): C, 43.01; H, 2.72; N, 4.72. Found: C, 43.20; H 2.74; N 4.61. IR υ_{max} (neat/cm^{-1}): 2026 (C≡O), 1926 (C≡O), 1893 (C≡O).

Synthesis of **$[Br(CO)_3Re(L)Pt(1,3$-dimethylbenzimidazol-2-ylidene$)]$** (**2d**)

In a round-bottom flask **[(L)Pt(1,3-dimethylbenzimidazol-2-ylidene)]** (40 mg, 0.057mmol) and **$Re(CO)_5Br$** (23 mg, 0.057 mmol) were dissolved in chloroform (5 mL). The reaction was refluxed overnight. After the reaction mixture has been cooled down to room temperature, chloroform was partially evaporated under reduced pressure and upon addition of cyclohexane the product precipitated which led after drying under vacuum to the pure product as an orange powder (56 mg, 0.054 mmol, 94 % yield). ^1H NMR ($CDCl_3$, 400 MHz, 298 K): δ 9.01 (d, $^3J_{H-H}$ = 5.1 Hz, 1 H, H^{19}), 8.70 (broad s, 1 H, H^5), 7.96 (t, $^3J_{H-H}$ = 7.4 Hz, 1 H, H^{17}), 7.70 (d, $^3J_{H-H}$ = 8.2 Hz, 1 H, H^{16}), 7.45-7.45 (m, 4 H, H^{10} + H^{18} + H^{22}), 7.35-7.41 (m, 3 H, H^{12} + H^{23}), 7.04 (d, $^3J_{H-H}$ = 8.6 Hz, 1 H, H^{13}), 6.67 (t, $^3J_{H-H}$ = 7.6 Hz, 1 H, H^{11}), 6.57 (dd, $^3J_{H-H}$ = 9.1 Hz, $^4J_{H-H}$ = 2.4 Hz, 1 H, H^4), 6.42 (d, $^4J_{H-H}$ = 2.4 Hz, 1 H, H^2), 4.27 (s, 6 H, NMe), 3.79 (s, 3 H, OMe). $^{13}C\{^1H\}$ Jmod NMR ($CDCl_3$, 100 MHz, 298 K): δ 195.2 (s, *C*≡O), 194.7 (s, *C*≡O), 169.5 (s, C^{14}), 168.7 (s, C^1), 164.6 (s, C^3), 161.7 (s, C^{20}), 156.2 (s, C^6), 153.1 (s, C^{19}), 150.2 (s, C^{15}), 148.6 (s, C^9), 140.0 (s, C^{17}), 135.2 (s, C^{11}), 134.8 (s, C^{21}), 129.7 (s, C^{10}), 124.4 (s, C^{18}), 123.9 (s, C^{13} + C^{23}), 117.0

(s, C^{11} +C^{16}), 110.5 (s, C^{22}), 110.0 (s, C^{8}), 106.6 (s, C^{4}), 104.2 (s, C^{7}), 103.9 (s, C^{2}), 55.4 (s, OCH$_3$), 33.8 (s, NCH$_3$). ^{195}Pt{^{1}H} NMR ($CDCl_3$, 86 MHz, 298 K): δ -2116 (s, Br(CO)$_3$Re(L2)*Pt*(NHC)). ESI-MS (MeCN) *positive mode exact mass* for $[C_{32}H_{24}N_6O_6BrPtReNa]^+$ (1072.0038): measured *m/z* 1072.0065 $[M+Na]^+$. Calcd for $C_{32}H_{24}N_6O_6BrPtRe$ (1049.8): C, 36.61; H, 2.30; N, 8.01. Found: C, 36.64; H 2.33; N 7.64. IR υ_{max} (neat/cm^{-1}): 2026 (C≡O), 1924 (C≡O), 1891 (C≡O).

Synthesis of **[(pyridine)(CO)$_3$Re(L)Pt(PPh$_3$)]BF$_4$** (**3c)**

In a round-bottom flask **[Br(CO)$_3$Re(L)Pt(PPh$_3$)]** (68 mg, 0.058 mmol) and **pyridine** (4.7 µL, 0.058 mmol) were dissolved in DCM (5 mL). **AgBF$_4$** (11 mg, 0.058 mmol) was dissolved in methanol (500 µL) and added onto the [Br(CO)$_3$Re(L2)Pt(PPh$_3$)]/pyridine mixture. The reaction was carried out at room temperature for 2 h. The reaction mixture was filtrated through celite, the solvent was evaporated and the product was washed with cyclohexane to lead after drying under vacuum to the pure product as an orange powder (48 mg, 0.039 mmol, 67 % yield). ^{1}H NMR (Acetone-d6, 400 MHz, 298 K): δ 9.32 (s, 1 H, H^{19}), 8.62 (d, $^3J_{H-H}$ = 3.8 Hz, 2 H, H^{24}), 8.43 (t, $^3J_{H-H}$ = 7.9 Hz, 1 H, H^{17}), 8.11 (t, $^3J_{H-H}$ = 7.3 Hz, 1 H, H^{26}), 7.95 (d, $^3J_{H-H}$ = 8.0 Hz, 1 H, H^{16}), 7.79-7.85 (m, 8 H, H^5 + H^{18} + H^{21}), 7.60-7.68 (m, 11 H, H^{22} + H^{23} + H^{25}), 7.43 (d, $^3J_{H-H}$ = 7.3 Hz, 1 H, H^{10}), 7.30 (t, $^3J_{H-H}$ = 7.3 Hz, 1 H, H^{12}), 6.58 (m, 2 H, H^{11} + H^{13}), 6.41 (m, 1 H, H^4), 5.95 (s, 1 H, H^2), 3.72 (s, 3 H, OMe). ^{31}P{^{1}H} NMR (Acétone-d6, 162 MHz, 298 K): δ 8.31 (t, $^1J_{P-Pt}$ = 4266 Hz, 1 P, PPh_3). Jmod NMR (CD_3CN, 100 MHz, 298 K): δ 195.2 (s, *C*≡O), 195.1 (s, *C*≡O), 170.4 (s, C^1), 170.1 (s, C^{14}), 165.6 (s, C^3), 157.6 (s, C^6), 154.1 (s, C^{19}), 153.7 (s, C^{24}), 150.7 (s, C^9), 151.3 (s, C^{15}), 143.8 (s, C^{17}), 141.6 (s, C^{26}), 136.5 (s, C^{12}), 135.3 (d, $^2J_{P-C}$ = 11.2 Hz, C^{21}), 133.3 (s, C^{10}), 132.4 (d, $^4J_{P-C}$ = 2.3 Hz, C^{23}), 129.5 (d, $^3J_{P-C}$ = 11.3 Hz, C^{22}), 128.4 (s, C^{25}), 128.3 (d, $^1J_{P-C}$ = 62.6 Hz, C^{20}), 127.3 (s, C^{18}), 125.2 (s, C^{13}), 119.2 (s, C^{16}), 117.9 (s, C^{11}), 109.9 (s, C^8), 107.9 (s, C^4), 105.1 (s, C^2), 103.6 (s, C^7), 55.7 (s, OCH$_3$). ^{195}Pt{^{1}H} NMR (Acetone-d6, 86 MHz, 298 K): δ -2440 (d, $^1J_{P-Pt}$ = 4281 Hz, [(pyridine)(CO)$_3$Re(L2)*Pt*(PPh$_3$)]$^+$). ESI-MS (MeCN) *positive mode exact mass* for $[C_{46}H_{34}N_5O_6PPtRe]^+$ (1165.1446): measured *m/z* 1165.1459 $[M-BF_4]^+$. Calcd for $C_{46}H_{34}N_5O_6PPtReBF_4.H_2O$ (1269.9): C, 43.51; H, 2.86; N, 5.52. Found: C, 43.40; H 2.94; N 5.35. IR υ_{max} (neat/cm^{-1}): 2037 (C≡O), 1923 (C≡O).

X-Ray crystal structure determination

For complex **1b**, a single crystal was selected, mounted onto a MiTeGen cryoloop and transferred into a cold nitrogen gas stream. Intensity data were collected with a Bruker Kappa APEX-II CCD diffractometer using a micro-focused Cu-Kα radiation (λ = 1.54178 Å). Data collection was performed at 140K with the Bruker APEXIII suite.[38] Unit-cell parameters determination, integration and data reduction were carried out with SAINT program.[38] SADABS was used for scaling and absorption correction.[39] The structure was solved with SHELXT[40] and refined by full-matrix least-squares methods with SHELXL[41] using Olex2 software package.[42] All non-hydrogen atoms were refined anisotropically. This structure was deposited at the Cambridge Crystallographic Data Centre with number CCDC 1971095 and can be obtained free of charge via www.ccdc.cam.ac.uk.

For complexes **2a** and **3c**, a single crystal of each compound was selected, mounted onto a MiTegen cryoloop and transferred into a cold nitrogen gas stream. Intensity data were collected with a Bruker Kappa APEX-II CCD diffractometer using a graphite-monochromated Mo-Kα radiation (λ = 0.71073 Å).

Data collections were performed at 200K with the Bruker APEXII suite.[38] Unit-cell parameters determinations, integrations and data reductions were carried out with SAINT program.[38] SADABS was used for scaling and absorption corrections.[39] The structures were solved with SHELXT[40] and refined by full-matrix least-squares methods with SHELXL[41] using Olex2 software package.[42] All non-hydrogen atoms were refined anisotropically. These structures were deposited at the Cambridge Crystallographic Data Centre with numbers CCDC 1971096 and 1971099 respectively and can be obtained free of charge via www.ccdc.cam.ac.uk.

For complex **2b**, a single crystal was selected, mounted onto a MiTeGen cryoloop and transferred into a cold nitrogen gas stream. Intensity data were collected with a Bruker Kappa APEX-II CCD diffractometer using a graphite-monochromated Mo-Kα radiation (λ = 0.71073 Å). Data collection was performed at 150K with the Bruker APEXII suite.[38] Unit-cell parameters determination, integration and data reduction were carried out with SAINT program.[38] TWINABS was used for scaling and absorption correction.[39] The structure was solved with SHELXT[40] and refined by full-matrix least-squares methods with SHELXL[41] using Olex2 software package.[42] The structure was refined as a 2-component twin with mass percentages of 73/27 around (Twin law: -100 0-10 001). All non-hydrogen atoms were refined anisotropically. This structure was deposited at the Cambridge Crystallographic Data Centre with number CCDC 1971097 and can be obtained free of charge via www.ccdc.cam.ac.uk.

For complex **2c**, a single crystal was selected, mounted onto a MiTeGen cryoloop and transferred into a cold nitrogen gas stream. Intensity data were collected with a Bruker Kappa APEX-II CCD diffractometer using a graphite-monochromated Mo-Kα radiation (λ = 0.71073 Å). Data collection was performed at 200K with the Bruker APEXII suite.[38] Unit-cell parameters determination, integration and data reduction were carried out with SAINT program.[38] SADABS was used for scaling and absorption correction.[39] The structure was solved with SHELXT[40] and refined by full-matrix least-squares methods with SHELXL[41] using Olex2 software package.[42] Molecules form large void areas in the crystal lattice. In these areas, unattributed residual electron density is present. It should be due to very disordered solvent molecules. A PLATON SQUEEZE procedure was applied on structure refinement to mask electron density of these very disordered solvent regions.[43] Crystal was obtained with a mixture of solvents, so it is impossible to identify and quantify which one are present in the crystal. Almost non-hydrogen atoms were refined anisotropically. Only the minor position of Br_1/C_5-O was refined isotropically because in anisotropic mode, anisotropic displacement parameters of these atoms became meaningless. This structure was deposited at the Cambridge Crystallographic Data Centre with numbers CCDC 1971098 and can be obtained free of charge via www.ccdc.cam.ac.uk

BDE calculations

Calculations were performed using the Gaussian 09 software package.[4] Optimization of geometries, frequency and single point energy calculations were done using the PBE0 functional[45] with the following basis set: SDD[46] for Pt and 6-31G(d,p) for others atoms.[47]

Cell culture and cell growth inhibition

Human breast cancer cell lines MCF7 and MDA-MB-231 were cultivated in DMEM (Dulbecco's Modified Eagle Medium) containing GlutaMaxI supplemented with 10% FBS and 1% kanamycin at 37 °C in a humidified atmosphere and 5% CO_2. Human ovarian cancer cells A2780 were cultured in RPMI1640 containing GlutaMaxI supplemented with 10% FBS and 1% kanamycin at 37 °C in a humidified atmosphere and 5% CO_2. Non-cancerous cell line MCF10A was maintained in DMEM:F12 (1:1) cell culture media, 5 % heat inactivated horse serum, supplemented with HEPES (20 mM), L-glutamine (2 mM), epidermal growth factor (20 ng/mL), hydrocortisone (500 ng/mL), cholera toxin (100 ng/mL), and insulin (10 µg/mL). Cell viability was evaluated by using a colorimetric method based on the tetrazolium salt MTT [3-(4,5- dimethylthiazol-2-yl)-2,5-diphenyltetrazolium bromide], which is reduced by viable cells to yield purple formazan crystals. Cells were seeded in 96-well plates at a density of 40000 cells/mL (100 µL per well). After overnight attachment, a dilution series of the compounds were added in the medium, and cells were incubated for a further 72 h. Stock solutions of the complexes were prepared in water for cisplatin and the platinum and bimetallic compounds in DMSO. The percentage of DMSO in the culture medium did not exceed 1%. After 72 h, the medium was removed and the cells were incubated with MTT solution in PBS (10 µL of a 5 mg/mL) for 2-3 h of incubation. The formed purple formazan crystals were dissolved in 100 µL of DMSO by thorough shaking, and the absorbance at 560 nm was read using a plate spectrophotometer (FLUOstar OPTIMA). Each test was performed with at least 3 replicates and repeated at least 3 times. The IC_{50} value is determined using GraphPad Prism 8.0 software.

Log $P_{o/w}$ determination by HPLC

Solutions of different compounds were prepared at 1 mM in MeOH. To 200 µL of these solutions, 10 µL of uracil solution (5 mM in MeOH) were added as internal standard and solutions were further diluted to a final concentration of 250 µM. Measurement of the octanol/water partition coefficient (log $P_{o/w}$) was done by HPLC technique according to the method previously described.[35] Measurement of the chromatographic capacity factors (k) for each molecule was done by varying the percentage of organic eluent (methanol containing 0.25% 1-octanol (v/v)) in the 98–60% range in the aqueous eluent (0.15% n-decylamine (v/v) in MOPS buffer pH 7.4 prepared in 1-octanol saturated water). These capacity factors (k') were extrapolated to 100% of the aqueous eluent, giving the value of k'_w. The log$P_{o/w}$ was obtained by the formula: Log Po/w = 0.31418 + 0.98452 log k'_w.

Determination of cellular content of **2a-d** and **3c** in MDA-MB-231 cells by transmission FT-IR spectroscopy

MDA-MB-231 cells were seeded in 75 cm^2 flasks at a density so as to reach confluency after 24 h. Cells were washed with 1×D-PBS and fresh growth medium (DMEM, 12 ml) containing **2a-d** and **3c** (50 µM in 1% DMSO) was added. Cells were incubated at 37 °C under a humidified atmosphere and 5% CO_2 for 2 h. At the end of the incubation, the medium was discarded and cells were washed with D-PBS. Trypsin (1× trypsin-EDTA, 0.05% trypsin, 0.53 mM EDTA, 2 ml) was added and cells were incubated 5 min at 37 °C in a humidified atmosphere and 5% CO_2. DMEM medium (8 ml) was added

to quench the action of trypsin. The suspension was centrifuged (520g, 5 min) and the supernatant discarded. After resuspension in D-PBS (100 µl), the number of cells was estimated by visual counting in a Malassez chamber (10 µl). A volume of D-PBS was added to reach ca. 10^5 cells per 10 µl. Another 10 µl of the suspension was diluted to 1/50 and cells were counted again in the Malassez chamber to determine the exact number of cells deposited on the nitrocellulose disks (6 mm-diameter). The disks were allowed to dry in air (ca.2 h). Experiments were done in triplicate for each concentration and for each concentration, two nitrocellulose disks were produced to check the reproducibility of the procedure. Transmission FT-IR spectra were recorded at 4 cm^{-1} with 48 scans and subtracted from the IR spectrum of a disk covered with control cells. The absorbance of the band at 2029 cm^{-1} was used for quantification using a calibration curve established by spotting solutions of **2a-d** and **3c** at known concentration in D-PBS containing 1 % DMSO on nitrocellulose disks.

Acknowledgements

The work was financially supported by Sorbonne Université and CNRS and was granted access to the HPC resources of the HPCaVe centre at UPMC-Sorbonne Université. B. B. thanks Aurélie Bernard, Claire Troufflard for their help for NMR analyzes and Dr. Cédric Przybylski for the HR-MS analyzes. B. B. thanks Dr. Patricia Forgez for providing A2780 and MCF-10A cells.

References

[1] B. Rosenberg, L. Vancamp, T. Krigas, *Nature*, **1965**, *205*, 698-699.

[2] R. Oun, Y. E. Moussa, N. J. Wheate, *Dalton Trans.,* **2018**, *47*, 6645-6653.

[3] (a) M. Fanelli, M. Formica, V. Fusi, Luca Giorgi, M. Micheloni, P. Paoli, *Coord. Chem. Rev.,* **2016**, *310*, 41-79. (b) L. Bai, C. Gao, Q. Liu, C. Yu, Z. Zhang, L. Cai, B. Yang, Y. Qian, J. Yang, X. Liao, *Eur. J. Med. Chem.,* **2017**, *140*, 349-382.

[4] D. Wang, S. J. Lippard, *Nat. Rev. Drug Discov.,* **2005**, *4*, 307–320.

[5] N. J. Wheate, S. Walker, G. E. Craig, R. Oun, *Dalton Trans.,* **2010**, *39*, 8113-8127.

[6] (a) G. Jaouen, A. Vessières, S. Top, *Chem. Soc. Rev.,* **2015**, *44*, 8802–8817. (b) A. Levina, A. Mitra, P. A. Lay, *Metallomics,* **2009**, *1*, 458–470. (c) C. Santini, M. Pellei, V. Gandin, M. Porchia, F. Tisato, C. Marzano, *Chem. Rev.,* **2014**, *114*, 815–862. (d) B.Bertrand, M. R. M. Williams, M. Bochmann, *Chem. Eur. J.,* **2018**, *24*, 11840-11851.

[7] L. P.H. Yang, S. J. Kea, G. M. Keating, *Drugs,* **2007**, *15*, 2211-2230.

[8] S. A. Loza-Rosas, A. M. Vázquez-Salgado, K. I. Rivero, L. J. Negrón, Y. Delgado, J. A. Benjamín-Rivera, A. L. Vázquez-Maldonado, T. B. Parks, C. Munet-Colón A. D. Tinoco, *Inorg. Chem.,* **2017**, *56*, 7788-7802.

[9] G. Dahm, E. Borré, C. Fu, S. Bellemin-Laponna, M. Mauro, *Chem. Asian J.,* **2015**, *10*, 2368-2379.

[10] J. Fernández-Gallardo, B. T. Elie, T. Sadhukha, S. Prabha, M. Sanaú, S. A. Rotenberg, J. W. Ramos, M. Contel, *Chem. Sci.,* **2015**, *6*, 5269-5283.

[11] B. Bertrand, A. Citta, I. L. Franken, M. Picquet,·A. Folda, V. Scalcon, M. P. Rigobello, P. Le Gendre, A. Casini, E. Bodio, *J. Biol. Inorg. Chem.* **2015**, *20*, 1005-1020.

[12] L. K. Batchelor, D. Orti, P. J. Dyson, *Inorg. Chem.,* **2019**, *58*, 2501-2513.

[13] M. Wenzel, E. Bigaeva, P. Richard, P. Le Gendre, M. Picquet, A. Casini, E. Bodio, *J. Inorg. Biochem.,* **2014**, *141*, 10-16.

[14] M. Wenzel, B. Bertrand, M-J. Heymin-Ondel, V. Comte, J. A. Harvey, P. Richard, M. Groessl, O. Zava, H. Amrouche, P. D. Harvey, P. Le Gendre, P. J. Dyson, M. Picquet, A. Casini, *Inorg. Chem.,* **2011**, *50*, 9472-9480

[15] (a) L. Boselli, M. Carraz, S. Mazères, L. Paloque, G. González, F. Benoit-Vical, A. Valentin, C. Hemmert and H. Gornitzka, *Organometallics*, **2015**, *34*, 1046-1055. (b) M. Wenzel, A. de Almeida, E. Bigaeva, P. Kavanagh, M. Picquet, P. Le Gendre, E. Bodio, A. Casini, *Inorg. Chem.,* **2016**, *55*, 2544–2557.

[16] (a) V. Fernández-Moreira, I. Marzo, M. C. Gimeno, *Chem. Sci.,* **2014**, *5*, 4434-4446. (b) A. Luengo, V. Fernández-Moreira, I. Marzo, M. C. Gimeno, *Inorg. Chem.,* **2017**, *56*, 15159–15170.

[17] (a) S. Clède, C. Policar, *Chem. Eur. J.,* **2015**, *21*, 942-958. (b) S. Hostachy, C. Policar, N. Delsuc, *Coord. Chem. Rev.,* **2017**, *351*, 172-188.

[18] N. Fischer-Durand, D, Lizinska, V. Guérineau, B. Rudolf, M. Salmain, *Appl. Organomet. Chem.,* **2019**, *33*, e4798.

[19] C. Policar, J. B. Waern, M.-A. Plamont, S. Clède,C. Mayet, R. Prazeres, J.-M. Ortega, A. Vessières, A. Dazzi, *Angew. Chem. Int. Ed.,* **2011**, *50*, 860-864.

[20] Y. Wang, F. Heinemann, S. Top, A. Dazzi, C. Policar, L. Henry, F. Lambert, G. Jaouen, M. Salmain, A. Vessieres, *Dalton Trans.,* **2018**, *47*, 9822-9833.[21] S. Garbe, M. Krause, A. Klimpel, I. Neundorf, P. Lippmann, I. Ott, D. Brünink, C. A. Strassert, N. L. Doltsinis, A. Klein, *Organometallics,* **2020**, *39*, 746-756.

[22] (a) S. Steinhauser, U. Heinz, H. Nick, K. Hegetschweiler, *Eur. J. Inorg. Chem.,* **2004**, 4177-4192. (b) F. Slowinski, O. B. Ayad, O. Ziyaret, C. Botuha, L. Le Falher, K. Aouane, S. Thorimbert, *Org. Lett.,* **2013**, *15*, 3494-3497.

[23] A. Massard, V. Rampazzi, A. Perrier, E. Bodio, M. Picquet, P. Richard, J.-C. Hierso, P. Le Gendre, *Organometallics,* **2012**, *31*, 947-958.

[24] M. Bouché, G. Dahm, A. Maisse-François, T. Achard, S. Bellemin-Laponnaz, *Eur. J. Inorg. Chem.,* **2016**, 2828-2836.

[25] H. Motschi, P. S. Pregosin, *Inorg. Chim. Acta,* **1980**, *40*, 141-146.

[26] L. C.-C. Lee, K.-K. Leung, K. K.-W. Lo, *Dalton Trans.,* **2017**, *46*, 16357-16380.

[27] S. Clède, F. Lambert, R. Saint-Fort, M.-A. Plamont, H. Bertrand, A. Vessières, C. Policar, *Chem. Eur. J.,* **2014**, *20*, 8714-8722.

[28] J. A. W. Sklorz, S. Hoof, N. Rades, N. De Rycke, L. Könczöl, D. Szieberth, M. Weber, J. Wiecko, L. Nyulászi, M. Hissler, C. Müller, *Chem. Eur. J.,* **2015**, *21*, 11096-11109.

[29] E. D. Olmon, P. A. Sontz, A. M. Blanco-Rodríguez, M. Towrie, I. P. Clark, A. Vlček, Jr., J. K. Barton, *J. Am. Chem. Soc.*, **2011**, *133*, 13718-13730.

[30] V. Fernández-Moreira, M. C. Gimeno, *Chem. Eur. J.,* **2018**, *24*, 3345-3353.

[31] (a) C. P. Newman, R. J. Deeth, G. J. Clarkson, J. P. Rourke, *Organometallics*, **2007**, 26, 6225-6233. (b) J. K. Muenzner, T. Rehm, B. Biersack, A. Casini, I. A. M. de Graaf, P. Worawutputtapong, A. Noor, R. Kempe, V. Brabec, J. Kasparkova, R. Schobert, *J. Med. Chem.,* **2015**, *58*, 6283-6292.

[32] K. Brandenburg, **1999**, DIAMOND. Crystal Impact GbR, Bonn, Germany

[33] H. Yao, G. He, S. Yan, C. Chen, L. Song, T. J. Rosol, X. Deng, *Oncotarget,* **2017**, *8*, 1913-1924.

[34] S. Salehi, A. S. Saljooghi, A. Shiri, *Eur. J. Pharmacol.,* **2016**, *781*, 209-217.

[35] D. J. Minick, J. H. Frenz, M. A. Patrick, D. A. Brent, *J. Med. Chem.,* **1988**, *31*, 1923–1933.

[36] B. Bertrand, M. A. O'Connell, Z. A. E. Waller, M. Bochmann, *Chem. Eur. J.,* **2018**, *24*, 3613-3622.

[37] (a) B. Bertrand, J. Fernandez-Cestau, J. Angulo, M. M. D. Cominetti, Z. A. E. Waller, M. Searcey, M. A. O'Connell, M. Bochmann, *Inorg. Chem.,* **2017**, *56*, 5728-5740. (b) F. Chotard, L. Dondaine, C. Balan, A. Bettaïb, C. Paul, P. Le Gendre, E. Bodio, *New J. Chem.,* **2018**, *42*, 8105–8112.

[38] Bruker, **2012**, APEX II / APEX III / SAINT. Bruker AXS Inc., Madison, Wisconsin, USA.

[39] Bruker, **2001**, SADABS / TWINABS. Bruker AXS Inc., Madison, Wisconsin, USA

[40] G. M. Sheldrick, *Act. Cryst. A*, **2015**, *71*, 3-8.

[41] G. M. Sheldrick, *Act. Cryst C*, **2015**, *71*, 3–8.

[42] O.V. Dolomanov, L.J. Bourhis, R.J. Gildea, J.A.K. Howard, H. Puschmann, *J.Appl. Crystallogr.,* **2009**, *42*, 339-341.

[43] A. L. Spek, *Act. Cryst. C,* **2015**, *71*, 9-18.

[44] Gaussian 09, Revision D.01, M. J. Frisch, G. W. Trucks, H. B. Schlegel, G. E. Scuseria, M. A. Robb, J. R. Cheeseman, G. Scalmani, V. Barone, B. Mennucci, G. A. Petersson, H. Nakatsuji, M. Caricato, X. Li, H. P. Hratchian, A. F. Izmaylov, J. Bloino, G. Zheng, J. L. Sonnenberg, M. Hada, M. Ehara, K. Toyota, R. Fukuda, J. Hasegawa, M. Ishida, T. Nakajima, Y. Honda, O. Kitao, H. Nakai, T. Vreven, J. A. Montgomery, Jr., J. E. Peralta, F. Ogliaro, M. Bearpark, J. J. Heyd, E. Brothers, K. N. Kudin, V. N. Staroverov, R. Kobayashi, J. Normand, K. Raghavachari, A. Rendell, J. C. Burant, S. S. Iyengar, J. Tomasi, M. Cossi, N. Rega, J. M. Millam, M. Klene, J. E. Knox, J. B. Cross, V. Bakken, C. Adamo, J. Jaramillo, R. Gomperts, R. E. Stratmann, O. Yazyev, A. J. Austin, R. Cammi, C. Pomelli, J. W. Ochterski, R. L. Martin, K. Morokuma, V. G. Zakrzewski, G. A. Voth, P. Salvador, J. J. Dannenberg, S. Dapprich, A.

D. Daniels, Ö. Farkas, J. B. Foresman, J. V. Ortiz, J. Cioslowski, D. J. Fox, Gaussian, Inc., Wallingford CT, **2009**.

[45] (a) J. P. Perdew, K. Burke, M. Ernzerhof, *Phys. Rev. Lett.,* **1996**, *77*, 3865-3868. (b) C. Adamo, V. Barone, *J. Chem. Phys.,* **1999**, *110*, 6158-6170.

[46] D. Andrae, U. Haeussermann, M. Dolg, H. Stoll, H. Preuss, *Theor. Chim. Acta*, **1990**, *77*, 123-141.

[47] W.J. Hehre, R. Ditchfield, J. A. Pople, *J. Chem. Phys.,* **1972**, *56*, 2257-2261.

Table of Content

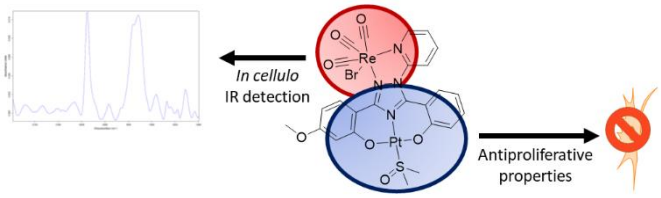

The development of heterobimetallic Pt(II)/Re(I) complexes offered tools for the optimization of the anticancer properties of a new Pt(II) scaffold bearing a (O^N^O) pincer ligand associated with a monodentate ligand.